2008

GAS SENSING PROPERTIES AND TRANSPORT PROPERTIES OF MULTI WALLED CARBON NANOTUBES

Raghu Mangu
University of Kentucky

Recommended Citation

Mangu, Raghu, "GAS SENSING PROPERTIES AND TRANSPORT PROPERTIES OF MULTI WALLED CARBON NANOTUBES" (2008). *University of Kentucky Master's Theses*. 578.
https://uknowledge.uky.edu/gradschool_theses/578

ABSTRACT OF THESIS

GAS SENSING PROPERTIES AND TRANSPORT PROPERTIES OF MULTI WALLED CARBON NANOTUBES

Multi walled carbon nanotubes (MWCNT) grown in highly ordered porous alumina templates were incorporated into a resistive gas sensor design and were evaluated for their sensitivities. The material characteristics and electrical properties of the nanotubes were analyzed. A study was undertaken to elucidate the effect of UV light on desorption characteristics and the dependence of sensitivity on (i) thickness of amorphous carbon layers and (ii) flow rates of analyte gases. These sensors were highly responsive to both oxidizing and reducing gases with steady state sensitivities of 5% and 10% for 100ppm of NH_3 and NO_2 respectively, at room temperature.

As part of a comparative study, thick films of MWCNTs grown on Si/SiO_2 substrates were integrated into various nano-composite based sensors and were evaluated for their response. Steady state sensitivities as high as 10% and 11% were achieved for 100ppm of NH_3 and NO_2 respectively, at room temperature.

MWCNTs were characterized for their electrical properties by I–V measurements at room temperatures. A typical I-V curve with an ohmic behavior was observed for a device with high work function metals (example: Au, Pt); Schottky behavior was observed for devices with metal contacts having low work functions (example: Al, Cu).

KEYWORDS: Porous Alumina, Multi Walled Carbon Nanotubes, CVD, Schottky contact, Gas Sensors

Raghu Mangu

02 Dec, 2008

GAS SENSING PROPERTIES AND TRANSPORT PROPERTIES OF MULTI WALLED CARBON NANOTUBES

By
Raghu Mangu

Dr. Vijay P. Singh

Director of Thesis

Dr. YuMing Zhang

Director of Graduate Studies

December 02, 2008

Name	Date

THESIS

Raghu Mangu

The Graduate School

University of Kentucky

2008

GAS SENSING PROPERTIES AND TRANSPORT PROPERTIES OF MULTI WALLED CARBON NANOTUBES

THESIS

A thesis submitted in partial fulfillment of the requirements for the degree of
Master of Science in Electrical Engineering in the College of Engineering
at the University of Kentucky

By
Raghu Mangu
Lexington, Kentucky
Director: Dr. Vijay P. Singh, Professor
Electrical and Computer Engineering
Lexington, Kentucky
2008

DEDICATION

To My Dad

ACKNOWLEDGEMENTS

A thesis is not conceivable without the support of a lot of people. I would like to express to everyone who contributed to this thesis my sincere gratitude. First of all I like to thank Dr. Vijay Singh. It was a pleasure to work in his group. His enthusiasm for new ideas, new collaborations, and also the work I did, always helped me with my thesis. I appreciated very much the freedom which I could enjoy during the two years of work in his group.

I am especially grateful to Dr. Suresh Rajaputra who taught me a lot about experimentation and the business of an experimentist. He also helped me a lot with his precise, very competent and professional advices. His well organized and efficient work impressed me very much.

I would also like to express my deep thanks to Dr. Todd Hastings and Dr. Janet Lumpp who has served on my thesis reading committee. Your expertise in this subject matter has helped me write a very high quality thesis.

Furthermore I like to thank Dr. Rodney Andrews and Dali qian at Centre for Applied Energy Research (CAER) for their support for the growth of carbon nanotubes. We had a very interesting and fruitful collaboration.

Especially, I am greatly indebted to my parents and my brother for their sacrifice during the tough time I had. Finally, my parents and my brother are always my firmest support through all of my life. I always love them.

Table of Contents

List of Tables

List of Figures

1. Introduction

1.1 Background and Motivation

Since the discovery of carbon nanotubes (CNTs) by Iijima in 1991[1], significant progress has been achieved for both understanding the fundamental properties and exploring possible engineering applications [2]. The gas sensing applications of carbon nanotubes in particular is very attractive. Due to their hollow centre, small size, high surface area, excellent mechanical and electronic properties, CNTs are ideal for gas sensing applications. CNT sensors are also sensitive to low vapor pressure species such as nerve agents, blister agent and explosives, species that are difficult to sense with conventional sensors [3].

Despite many attractive features, commercial solid state device gas sensors do have some drawbacks which impede their performance. The common problems of the solid state devise gas sensors are stability, reproducibility, selectivity and sensitivity [4]. However, the objective of this dissertation was to overcome one of the major disadvantages of gas sensors, i.e., sensing at elevated temperatures. Most of the other solid state devise are operated at 200 to 600ºC thus having an in-built heater thereby increasing the power consumption and the design complexity of the sensor device. A nanosensor technology was developed using multi walled carbon nanotubes (MWNTs) with an Anodized Aluminum Oxide (AAO) template based fabrication and also silicon-based fabrication. This technology provides a sensor that can accommodate a number of nanotubes with the advantages of high sensitivity, low power consumption, compactness, high yield and low cost for specific applications like in-situ chemical analysis in space and terrestrial applications. This platform is suitable for detection of gases, chemical analysis in gas phases, and volatile organic compounds.

In the past, many researchers have reported on using individual, network films, or bundles of CNTs for both capacitive and resistive sensors [5-9]. However, integrating individual or bundles of CNTs into a sensor design often involves cumbersome and expensive processing steps. The fabrication process of our resistive sensors is simple and does not require any manipulation of individual or bundles of tubes, or any techniques such as e-beam or photolithography. Several studies have been conducted on non-aligned Carbon nanotube based chemical sensors [11-21], which were designed to operate when gas molecules are adsorbed on the outer walls of CNTs. In our device configuration, the MWCNTs are open ended on both sides, which allows the gas molecules to permeate through the tubes and adsorb on the inner walls. Other researchers have fabricated CNT arrays in AAO templates [7-9, 11-13, and 22-24]. We are the first group to develop a resistive sensor design based on embedded MWCNTs and obtain high sensitivities to low concentrations of NH_3 and NO_2 gases. Our design also provides for a large well-defined surface area and the capacity for modifying the carbon nanotube surface with various transduction materials [17, 22-24] to effectively enhance the sensitivity and broaden the scope of detectable analytes. Further, the sensor response can be tuned by controlling the diameter and the density of nanotubes; this can be accomplished by varying the pore size and inter-pore spacing in the starting AAO templates [25] and the CVD process conditions [26].

Carbon nanotubes are being investigated as active materials for building nano-electronic devices, such as, the carbon nanotube field effect transistors (CNTFETs) [27, 28] and CNT diodes [29–35]. Diode like rectification across a CNT has been achieved by forming a *p-n* junction through chemical doping,[29, 30] polymer coating,[31] impurities,[32] or intramolecular junctions.[33] In addition, the *p-n* junction were manipulated by electrical gating using AFM tip scanning probe [34] or by using a pair of split gates[35]. The reported CNT diodes to date have mostly focused on *p-n* junctions instead of metal/ semiconductor Schottky junctions. It was only very recently that Manohara *et al.*[36] has reported the use of Pt and Ti contacts to form CNT Schottky diodes. The objective of this study was to demonstrate a Schottky diode formed at the interface of a metal and the semiconducting carbon nanotube.

1.2 Objective

The feasibility of integrating Multiwall carbon nanotubes into different resistive sensor designs has not been demonstrated in past research. The objectives of this research work were:

- To investigate different device configurations for MWCNT sensors.
- To investigate gas sensing properties of MWCNT sensors for both oxidizing and reducing gases.
- To demonstrate the dependence of the device sensitivity on various factors like thickness of amorphous carbon and flow rate of the test gas.
- To investigate the electrical properties by various characterization techniques like Voltage – Current and Voltage – Capacitance measurements.
- To determine any difficulties associated with MWCNT device integration, and find solution to any potential problems.

1.3 Contributions

The main contributions of this dissertation were:

- The dependence of the thickness of amorphous carbon layer on the device sensitivity was extensively studied and this explained why previous CNT-based sensors exhibited in poor sensitivities.
- MWCNTs embedded in highly ordered AAO membranes were characterized for their electrical properties by Current – Voltage (I–V) measurements at room temperature for various metal contacts.
- MWCNT – Polymer and MWCNT – Nano crystalline composite sensors were developed which showed high sensitivities on exposure to analyte gases.
- A major difficulty associated with handling of AAO membrane based MWCNT sensor devices was identified and a partial solution of using substrate based devices was proposed.

1.4 Organization of the Dissertation

Chapter 2.1 gives an introduction to carbon nanotubes based sensor devises, their configuration advantages and other sensor issues. Chapter 2.2 introduces to the electronic applications of carbon nanotubes and their performance related issues. Chapter 3.gives detailed procedures for different fabrication and characterization techniques of all the MWCNT based devices studied in this dissertation. The chapter begins with fabrication procedures and then different characterization techniques are introduced. The sensor measurement methodology is also presented. Chapter 4 gives results of different characterization techniques. The current – voltage measurements are explained elucidately. The sensor responses of all the nanotube based devices are also discussed extensively. Chapter 5 gives conclusions drawn from the research and directions for the future work.

2. Carbon nanotubes

2.1 Overview of Carbon nanotubes

Carbon nanotubes (CNTs) were discovered in 1991 by S. Ijiima [37]. They are molecular-scale one dimension tubes of graphitic carbon with some unique properties and can be divided into two categories, namely the single-walled carbon nanotubes (SWNTs) and the multi-walled nanotubes (MWNTs). A single-walled carbon nanotube is a sheet of graphite rolled into cylinder with high aspect ratio. Its diameter in the order of nanometers and its length may vary from tens of nanometers to few millimeters. A multi-walled CNT is similar to single-walled CNTs but has more than one rolled sheet in the cylinder.

CNTs possess very unique characteristics such as high Young's modulus [38], and they can behave either as metallic or semi conductive material depending on their diameter and chirality [39]. Potential applications of CNTs include cold cathode flat panel display (FPD) [40], microelectronic devices [41], tips for scanning probe microscopes [42], hydrogen storage [43], quantum wires [44], and high power electrochemical capacitors [45]. In addition, CNT-based gas sensors for methane [46], oxygen [47], carbon dioxide [48], and ammonia [49] detection have been reported.

Some of the many electrical properties experimentally investigated in CNTs are, e.g., the band structure [50], single charging effects [51], Kondo effect [52], ballistic conduction [53], proximity-induced [54] and intrinsic superconductivity [55], 1/f-noise [56] and Luttinger-liquid phenomena .

Due to their unique molecular structure, CNTs are one of the stiffest and strongest materials [57], they are one of the most effective thermal conductors [58] and also have many novel electrical and optical properties. These unique characteristics make CNTs potentially useful in a wide variety of applications in nanotechnology, sensors, actuators, electronics and optics. A CNT can be either metallic or semiconducting, the chirality being the key to this electric property, Fig 2.2 illustrates chirality which is represented by a pair of indices ($n;m$) called the chiral vector [59]. The integers n and m denote the number of unit vectors along two the directions in the honeycomb crystal lattice of graphene. If $m = 0$, the nanotubes are “zigzag" and if $n = m$, the nanotubes are “armchair". Otherwise, they are called “chiral". In a SWNT, if (n ¡ m) is multiple of 3, then it is metallic, otherwise it is semiconducting.

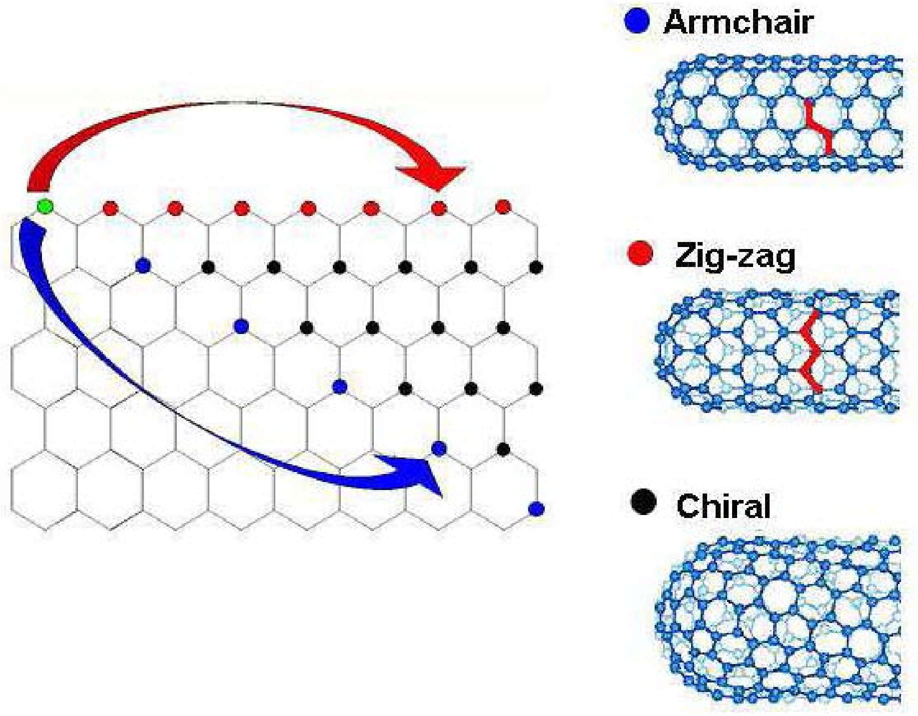

Figure 2.1: Chirality in carbon nanotubes. Imagine the hexagonal lattice being rolled such that the green dot (carbon atom) matches up with another colored atom. Each color (red, blue, black) corresponds to a different structure [60].

2.2 Carbon Nanotube based Sensors

Gas detection instruments are increasingly needed for industrial health and safety, environmental monitoring, and process control. To meet this demand, considerable research into new sensors is underway, including efforts to enhance the performance of traditional devices, such as resistive metal oxide sensors, through Nano Engineering. Metal oxide sensors have been utilized for several decades for low-cost detection of combustible and toxic gases. However, issues with sensitivity, selectivity, and stability have limited their use, often in favor of more expensive approaches. Recent advances in nanomaterials provide the opportunity to dramatically increase the response of these materials, as their performance is directly related to exposed surface volume. The recent availability of various metal oxide materials in high-surface-area nanopowder form, as well as implementation of newly developed nanofabrication techniques, offer tremendous opportunities for sensor manufacturers.

Recently, it has been demonstrated that CNTs represent a new type of chemical sensor capable of detecting a small concentration of molecules, such as CO, NO_2, NH_3, etc. [61]. Exchange of electrons due to absorption of gas molecules on the CNTs causing a modification of the electrical conductance in the nanotubes is the basic concept for high sensitively molecular sensor based CNTs. Also, the ballistic electronic transport along the CNT axis provides excellent transmission of the altered electrical signal to the external contact. Third, the long-term performance of CNTs based sensor may be stable due to their chemically robust graphitic surface.

Several researchers have reported on the fabrication of CNT arrays and AAO templates [62, 63] Some groups have used an external catalyst particle (Co, Fe or Ni) deposited at the bottom of the AAO template to grow CNT arrays, while others have used the AAO itself as a catalyst. The latter method is preferable because then one of the ends of the tube is not capped by the external catalyst particle. Also, the chemical purity of the nanotubes can be compromised by the catalyst particles. In this research we report fabrication of MWCNTs in free standing AAO templates without the use of a catalyst, AAO itself acting as a catalyst.

The effect of gas adsorption on the electrical resistance of a CNT has received great attraction because of fast response, good sensitivity of chemical environment gases and low operating temperature [64]. Theoretical studies have confirmed the remarkable change in electronic properties of CNT due to the detection of gas molecules [65]. Most molecules are known to be an electron-acceptor such as NO_2 and O_2 or an electron donor such as NH_3 and H_2O displaying relatively small charge transfer between adsorbed molecules weakly on the CNT wall. Multiwalled carbon nanotube (MWCNT) thin films show p-type semiconducting property of decreasing resistance upon exposure of NO_2 gas [66, 67]. CNT sensors require some external agitation like thermal-heat or an electric pulse or high energy UV light to desorb the chemisorbed molecules from the surface. The sensor exhibits variation of the electrical resistance of CNT films in the adsorption–desorption cycles and reproducible recovery in the operating temperature range of 25–250°C [66-68].

2.3 Carbon Nanotube Transport Mechanism

The Schottky diode fundamentally operates differently to a *p-n* diode. The reverse current of a *p-n* diode arises from minority carriers diffusing through the depletion layer, and the forward current is due to minority carrier injection from *n* and *p* sides. On the other hand, the Schottky diode's reverse current is due to carriers which overcome the barrier, and the forward current is due to majority carrier injection from the semiconductor; this leads to diode devices with a small threshold voltage [69].

However, there is often a controversy between the observed electrical transport properties and a simple band picture in the measurements, where carbon nanotube is contacted to metal electrodes. This is due to the lack of control and understanding of the role of the metal contacts that play a significant role in the transport properties [70]. Also impurities and surfactants on the tube often break down the ideal picture in practical experiments [71].

Metal-semiconductor junctions play very important roles in electronic devices. Nanoscale CNT devices rely upon the fundamental understanding of the CNT-metal interface.

Fermi level pining at the metal-nanotube interface is weak, so a range of Schottky barrier heights can be achieved by using different contact metals. This thesis work reports the behavior of the nanotube with various metal interfaces. The conduction and valence bands of the CNTs are symmetric, which is advantageous for complementary applications. The band structure is direct, which enables optical emission, and finally, CNTs are highly resistant to electromigration. Significant efforts have devoted to understand how a carbon nanotube transistor operates and to improve the transistor performance [72]. It has been demonstrated that most CNTFETs to date operates like non-conventional Schottky barrier transistors [73], which results in quite different device and scaling behaviors from the MOSFET-like transistors [74]. Important techniques for significantly improving the transistor performance, including the aggressively scaling of the nanotube channel, integration of thin high-κ gate dielectric insulator [75], use of excellent source/drain metal contacts [76], and demonstration of the self-align techniques, have been successfully developed. Very recently, a nanotube transistor, which integrates ultra-short channel, thin high-κ top gate insulator, and excellent Pd source/drain contact is demonstrated using a self-align technique [77]. Promising transistor performance exceeding the state-of-the-art Si MOSFETs is achieved.

CNT FETs built from as-grown CNTs are found to be either *p* type, or ambipolar. This behavior has been attributed to the presence of a Schottky barrier at the metal-nanotube contact [78]. Most of the reported CNT FET use symmetrical CNT-metal contacts, i.e., the same elemental metal contact on both terminals of the CNT channel [79, 80]. In this work, we demonstrate the CNT Schottky diode formed with different metal interfaces and extensively study their behavior.

3. Experimental Procedures

3.1 Fabrication Procedures

3.1.1 Fabrication of AAO templates

Nowadays, porous alumina is one of the most prominent template materials for synthesis of nanowires or nanotubes with mono disperse controllable diameter and high aspect ratios. In an anodizing cell, the aluminum work piece is made the anode by connecting it to the positive terminal of a dc power supply. The cathode is connected to the negative terminal of the supply. The cathode is a plate of platinum which is unreactive (inert) in the anodizing bath. When the circuit is closed, electrons are withdrawn from the metal at the positive terminal, allowing ions at the metal surface to react with water to form an oxide layer on the metal. The electrons return to the bath at the cathode where they react with hydrogen ions to make hydrogen gas. (See the Appendix for the chemical reactions occurring during this process.)

Bath electrolytes are selected in which the oxide is insoluble, or dissolves at a slower rate than it deposits, and then an adherent oxide layer grows. The bath composition is the primary determinant of whether the film will be barrier or porous. Barrier oxide grows in near neutral solutions in which aluminum oxide is hardly soluble, most commonly ammonium borate, phosphate, or tartrate compositions. Porous oxide grows in acid electrolytes in which oxide can not only be deposited but also dissolves. The most widely used bath is dilute sulfuric acid, typically about 1 molar or 10 weight percent concentration. Other baths used for particular applications are made with oxalic acid or phosphoric acid.

Since the formation of pores in AAO depends directly on the existing electric field between the electrodes, it can be inferred that the current density at the electrodes is decided by the porosity of the alumina membranes. Hence for the purpose of fabricating AAO with varying pore diameters and inter-pore distances, two different means (galvanostatic and potentiostatic) of anodizations were selected. However, most of the samples used in this research were fabricated by means of a standard potentiostatic anodization technique. Additionally, the effect of various electrolytes and anodizing potentials on the pore diameters and inter-pore spacing were also studied.

Highly aligned standard porous alumina templates used in this research work for growing MWCNTs in them were prepared by anodizing high purity Aluminum tape in a 0.3M oxalic acid medium at 40V. A piece of aluminum tape measuring 1 in. on each side and 60µm thick was first cut from a high purity aluminum tape roll. It was then immersed in methanol solution and sonicated at high frequencies for a couple of minutes, followed by rinsing with de-ionized water. A second round of sonication with acetone was done followed by rinsing with de-ionized (DI) water and drying with Nitrogen. Substrates thus prepared ensured that the surface was thoroughly cleaned and were subsequently used for the Anodization procedure as detailed by Knaack, Redden and Onellion **[**80**]**.

The Anodization process is performed in a cell where a Platinum sheet measuring 1” x 1” was used as the cathode while the substrates were made the cathode. The whole setup was immersed in a 0.3M oxalic acidic bath which was continuously stirred at 60 rpm and the voltage was supplied using a Kepco (Model ABC 125-1DM) programmable constant DC power supply. A cleaned specimen was then anodized in the above setup at 4-5^0C at the constant applied voltage of 40 V for ten minutes. And then aluminum oxide film was subsequently removed by dipping the anodized specimen into a mixture of phosphoric acid (5 wt.%) and chromic acid (10 wt.%) at 85^0C. A second step Anodization was performed for 22 hours under the same condition as the first one. The pore depth was approximately 60 µm. The pore diameter was ranging from 40nm to 50nm.

The sensor response can be tuned by controlling the diameter and the density of nanotubes; which is achieved by varying the pore size and inter-pore spacing of the starting AAO templates Thus, the effect of various anodization voltages on the pore diameter and inter pore spacing were carefully investigated by using two different electrolytes i.e. 10% vol. H_2SO_4 and 10% vol. H_3PO_4 acid bath solutions respectively. Six different anodization conditions were tried as shown in table 3.1 and are discussed in detail in the next section.

Electrolyte	**Anodization Voltage**
10% vol. H_2SO_4	5 volts
10% vol. H_2SO_4	15 volts
10% vol. H_3PO_4	20 volts
10% vol. H_3PO_4	60 volts
10% vol. H_3PO_4	80 volts
10% vol. H_3PO_4	120 volts

Table 3.1: Various potentiostatic anodization conditions investigated.

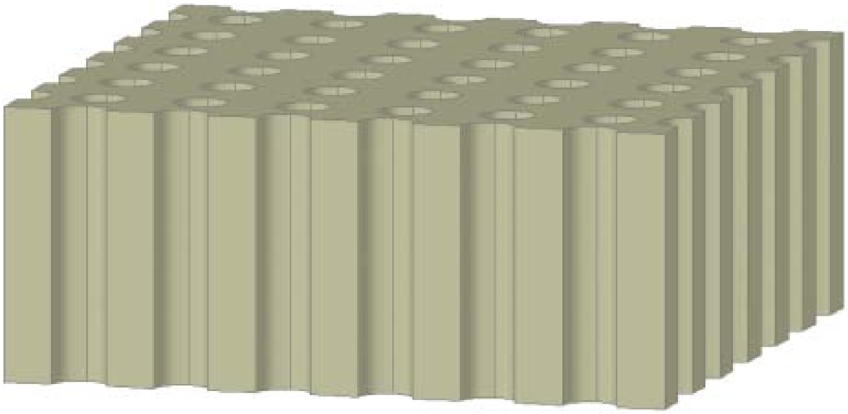

Fig 3.1 Schematic of a porous AAO template with pores open at both the ends

To ensure a clean top surface and uniform pore distribution, a two-step Anodization process was performed. All the anodization processes were continuously monitored for variations in current with respect to elapsed time by the application of software developed in-house using LabVIEW 7.0 student edition provided by National Instruments. The templates after the two-step Anodization process were thoroughly rinsed in DI water and were dried using Nitrogen flush. These templates were then immersed in Acetone for 24 hours to remove the backing paper and glue. A thin layer of un-anodized aluminum was left at the back side of the template which was removed by chemical etch using a mixture Cupric Chloride and HCL. The templates were immersed in the acid solution for four hours to make sure that the aluminum was completely etched off. The templates thus obtained had a thin barrier layer (30nm) at the bottom which was removed by floating the templates on 5% Phosphoric (H_3PO_4) acid (such that the BL side faces the acid) for 2 minutes at 60^oC. Finally the templates were thoroughly rinsed in DI water and annealed for 2 hours at 750^oC in a Lindburg furnace where oxygen was continuously purged at a rate 800sccm.

3.1.2 Fabrication of porous alumina films on silicon substrates

P-type silicon wafers were used as starting substrates for fabricating thin porous alumina films. Thick oxide layer (200nm) was grown by thermal Oxidation of these wafers in a Lindburg high temperature oxidation furnace. The wafers were RCA cleaned prior to the oxidation process and were loaded into the furnace at an ambient temperature of 800^oC and then the furnace was set to an oxidation temperature of 1100^oC. Nitrogen gas was purged in the oxidation chamber at a rate of 1000sccm.for more than 30minutes prior to loading the sample to reduce the risks of contamination. The typical gas flow rate of Oxygen was about 500 sccm once the oxidation temperature was attained. Thermal oxidation was performed for 30minutes followed by post oxidation annealing in Nitrogen gas flowing at 1000sccm for 2 hours. The theoretical calculation of the oxide thickness (200nm) was in agreement with the ellipsometry measurements.

A thin layer of titanium was used as an under layer for better adhesion of the aluminum film onto the SiO_2 surface. A MAXTEK single target sputtering machine was used to deposit 20nm thick titanium at a base pressure of 0.03 mille Torr. The oxidized silicon wafers were left for a two hour pump down cycle in the deposition chamber for obtaining the desired base pressure and then Argon gas was purged at a rate of 25 sccm. The thickness of the layer and the rate of deposition were controlled by a TM-100 MAXTEK crystal monitor by programming it with the density, thickness of deposition and the Z-ratio of titanium metal prior to the deposition. Next, a thin film of aluminum was deposited using Torr International E-Beam Evaporator via high-vacuum at a base pressure of 8.8×10^-6 Torr. The density (2.70 g/cm^3) and Z-ratio (1.080) of Aluminum were programmed in the system prior to the deposition. The source had a graphite crucible filled with Aluminum pallets. The samples were at distance of about 15cm from the source and the shutter was completely closed for the first few nanometers of Aluminum deposition. A supply voltage of 8KV was applied and the supply of current to the source was incremented slowly till the Al started melting (at RMS current value of 0.05Amps). Now the shutter was slowly opened to allow a controlled rate of Aluminum deposition. A 500nm-thick Al film was deposited with a deposition rate of 1Å/sec on the sample.

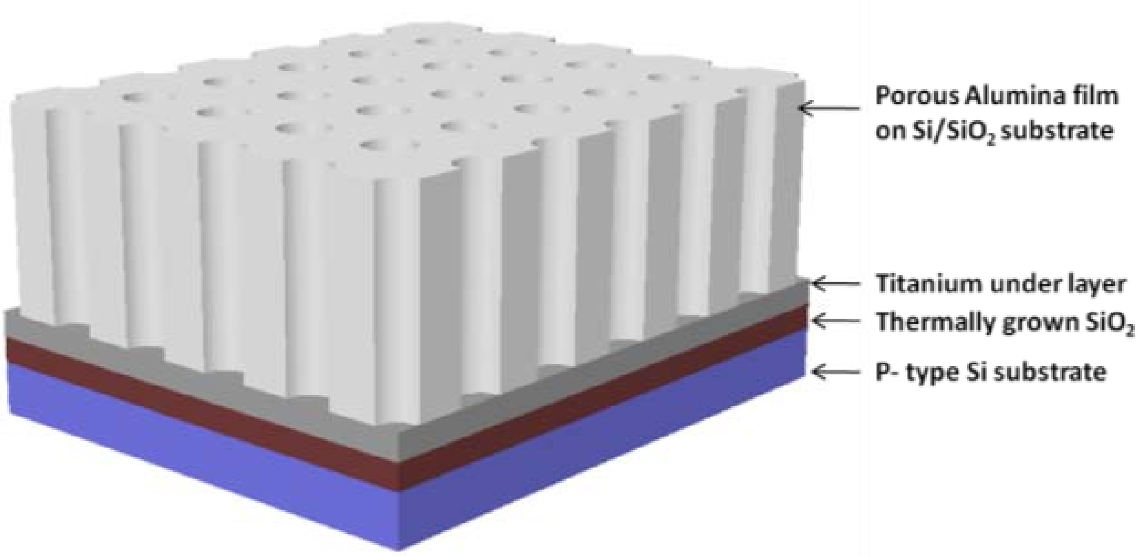

Fig 3.2 Schematic of a porous AAO template on Si/SiO$_2$ substrate

These samples were then anodized similar to the method described in section 3.1.1 to form well ordered pores of alumna with the pore diameter varying from 40 - 45nm.

3.1.3 Fabrication of CNTs in AAO templates by CVD

Chemical Vapor Deposition (CVD) is a widely used method for depositing thin films of a large variety of materials. Applications of CVD range from the fabrication of microelectronic devices to the deposition of protective coatings. In a typical CVD process, reactant gases (often diluted in a carrier gas) at room temperature enter the reaction chamber. The gas mixture is heated as it approaches the deposition surface, heated radiatively or placed upon a heated substrate. Depending on the process and operating conditions, the reactant gases may undergo homogeneous chemical reactions in the vapor phase before striking the surface. The porous alumina templates fabricated by the above mentioned procedure were used to grow vertically aligned multi walled carbon nanotube arrays by a chemical vapor deposition (CVD) method. The CVD process is similar to that described previously [81] except that in our method, pure xylene [$C_8H_{10}(C_6H_4C_2H_6)$] was used as hydrocarbon source and a stream of argon/hydrogen was replaced with nitrogen gas. The synthesis was carried out using a CVD system based on 96 mm diameter Lindberg furnace, with a specially designed gas-flow injector to minimize turbulent flow. The growth procedure was as follows: First the sample was heated to 700^{o}C where nitrogen was purged at 675 sccm over the course of 1 hour. Next, xylene was injected at the rate of 30ml/hr into the preheater (maintained at 250^{o}C) using a syringe pump for the first two minutes. As the xylene vapors emerged at the outlet of the preheater, the rate of Xylene injection was reduced to 1ml/hr for the whole CVD process. The stream of nitrogen gas swept the Xylene vapors into the furnace (maintained at 700^{o}C) where xylene decomposed to produce Carbon nanotubes within the AAO pores without the use of catalyst. The growth of nanotubes was performed for 1 hour by Xylene pyrolysis. The sample was then allowed to slowly cool in nitrogen.

A thin layer of amorphous carbon is formed on both sides of the template as a bi-product of the CVD process whose thickness can by controlled by either tailoring the CVD growth conditions or by post growth processing. During the CVD growth process, the thickness was tailored by regulating the flow of nitrogen and temperature in the furnace after the growth process. Tailoring the a-C layer thickness by post growth processing involves Oxygen plasma oxidation technique. A custom made microwave plasma oxidation apparatus was used for this procedure. The Sample was placed in the plasma chamber and evacuated to a vacuum pressure of 30 milli Torr. Oxygen gas was then carefully purged into the chamber by through a precision gas flow controller. The microwave was set to 60% power and the plasma oxidation was carried out for 2 minutes. The chamber was then allowed to cool for 30 minutes and then brought to atmospheric pressure and the sample was examined by Scanning Electron Microscopy and the removal of a-C layer was confirmed.

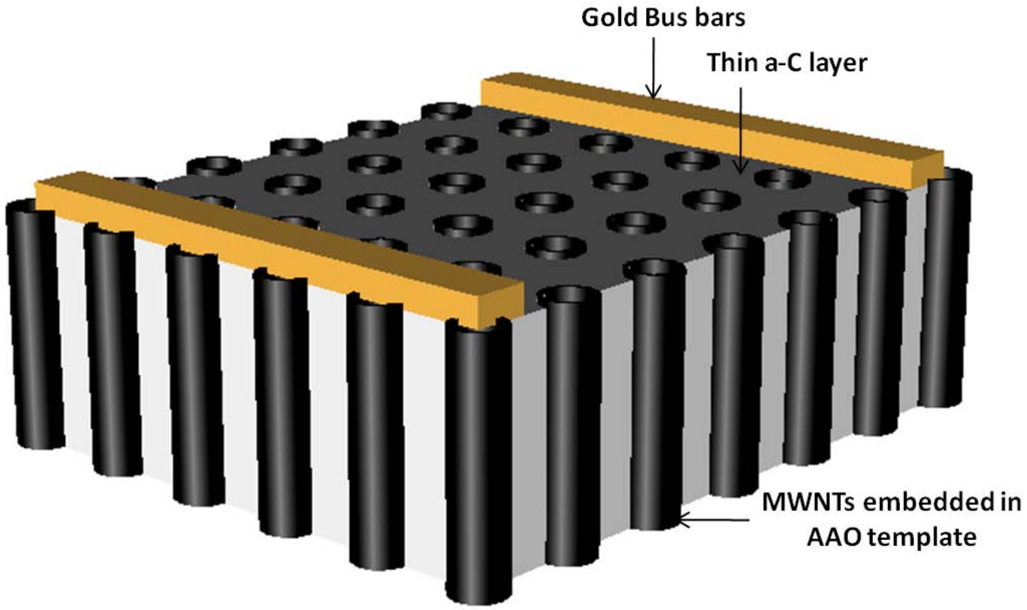

Fig 3.3 Schematic of free standing AAO template based Resistive Sensor design

3.1.4 Fabrication of CNTs on Silicon substrates by CVD

Free standing porous alumina templates with Multi walled Carbon nanotubes embedded in them were integrated into resistive sensor design. These devises were difficult to handle and had unique sensor characteristics. Thus CNTs were grown as thick films on Silicon substrates which were robust in design and easy to handle. P-type silicon wafers with a thick oxide grown form the substrates for these devises. Thermal Oxidation was performed on these wafers in a Lindburg high temperature oxidation furnace and a 200nm thick oxide layer was grown. The wafers were RCA cleaned prior to the oxidation process and were loaded into the furnace at an ambient temperature of

800^{o}C and then the furnace was set to an oxidation temperature of 1100^{o}C. Nitrogen gas was purged in the oxidation chamber at a rate of 1000sccm.for more than 30minutes prior to loading the sample to reduce the risks of contamination. The typical gas flow rate of Oxygen was about 500 sccm once the oxidation temperature was attained. Thermal oxidation was performed for 30minutes followed by post oxidation annealing in Nitrogen gas flowing at 1000sccm for 2 hours. The theoretical calculation of the oxide thickness (200nm) was in agreement with the ellipsometry measurements.

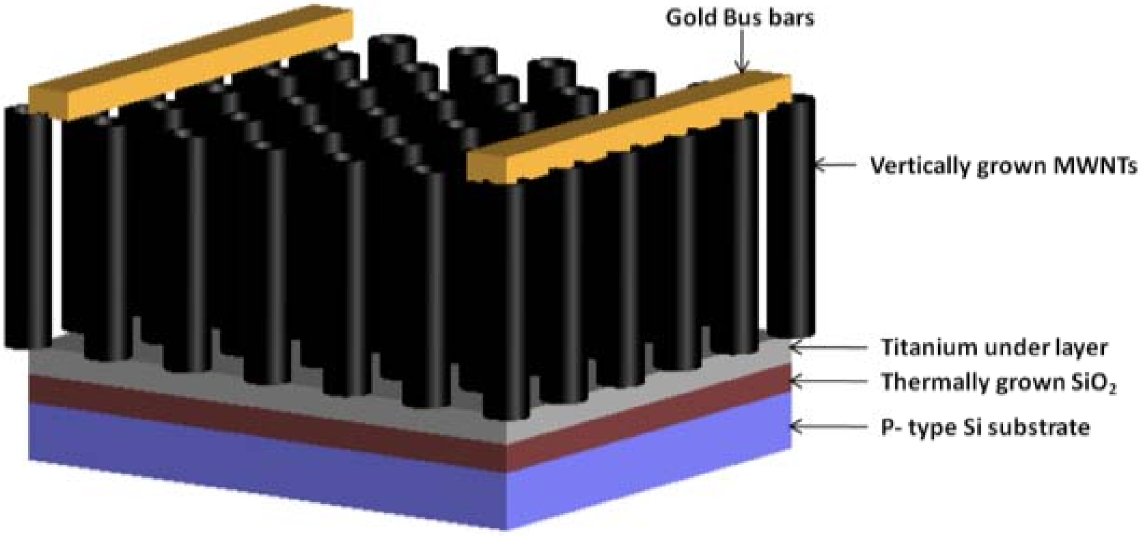

Fig 3.4 Schematic of MWNT based Resistive Sensor design with MWCNTs grown on Si/SiO$_2$ substrates.

Multiwalled Carbon Nanotubes were grown on these substrates by CVD catalysis where the synthesis was carried out in 96 mm diameter Lindberg furnace similar to the arrangement used to fabricate aligned nanotubes in AAO templates. The growth procedure was different with the use of Ferrocene [$Fe(C_5H_5)_2$] as a catalyst. Argon was purged at the rate of 675 sccm in the chamber until the temperature reached 800^{o}C. Next, Hydrogen purge was started at the rate of 75 sccm. Care was taken to maintain the Argon-Hydrogen ratio as 9:1 in the chamber for ideal catalytic reaction. A Ferrocene-Xylene mixture mixed in the ratio of 1:0.1148 (100gms of Xylene to 11.48gms of Ferrocene) was injected at the rate of 30ml/hr into the preheater (maintained at 250^{o}C) using a syringe pump for a duration of 130 seconds. As the vapors emerged at the outlet of the preheater, the Xylene-Ferrocene injection rate was reduced to 3ml/hr for the whole CVD process. The growth process was performed for 15 minutes and the hydrogen purge was stopped immediately. The samples were then allowed to slowly cool in flowing Argon.

3.1.5 Fabrication of thin film CNT – polymer composites

PEDOT:PSS obtained from Aldrich was spin coated on devices with CNT films grown on the Si-SiO_2 as explained in section 3.1.3. Chemat technology spin coater was used to spin coat PEDOT:PSS at 4000rpm for 40 seconds on these samples. The spin coated samples were then annealed in a Lindburg furnace in Argon environment for 2 hours at 100^oC. Argon was continuously purged at the rate of 300 sccm into the annealing furnace. Annealing removes the excess water molecules in the PEDOT:PSS layer on the sample and also increases the adhesion between the PEDOT:PSS and CNTs. The samples were left for about 2 hours to cool down to room temperature.

3.1.6 Fabrication of thin film CNT – nanocrystalline composites

0.01M TiO_2 solgel was spin coated on devices with CNT films grown on the Si-SiO_2 as described in section 3.1.3. Chemat technology spin coater was used to spin coat PEDOT:PSS at 4000rpm for 40 seconds on these samples. The spin coated samples were then annealed in a Lindburg furnace in Oxygen environment for 2 hours at 100^oC. Oxygen was continuously purged at the rate of 300 sccm into the annealing furnace. Annealing helps in removing the excess IPA in the solgel and also aids in making a better oxide of titanium. The samples were left for about 2 hours to cool down to room temperature.

3.1.7 Deposition of electrodes and integration of CNT based devices

For gas sensing experiments, MWCNTs with 25 nm inner core diameter and wall thickness of 5 nm were incorporated into a resistive gas sensor design (Fig.3.3), where, contact electrodes (Au bus bars) were deposited by e-beam evaporation technique using Torr International E-Beam Evaporator via high-vacuum at a base pressure of 8.8×10^-6 Torr. The samples were covered with a shadow mask of two bus bars measuring 0.2cm X 2cm in dimensions made from an aluminum foil sample. The density (2.70 g/cm^3) and Z-ratio (1.080) of Aluminum were programmed in the system prior to the deposition. The graphite crucible was filled with Gold pallets and the shutter was completely closed for the first few nanometers of Gold deposition. A supply voltage of 8KV was applied and the supply of current to the source was incremented slowly till the Au started melting (at RMS current value of 0.05Amps). Now the shutter was slowly opened to allow a controlled rate of metal deposition. A 100nm-thick Au film was deposited with a deposition rate of 1Å/sec on the sample.

Similarly, MWNCNTs embedded in porous alumina film on Si/SiO_2 substrates, MWCNT films grown on Si/SiO_2, MWCNT polymer and nanocrystalline composites on Si/SiO_2 and MWCNT polymer composite films on ITO glass substrates were also integrated into Resistive Sensor design by depositing Gold contact electrodes by E-beam evaporation technique.

For transport mechanism studies, MWCNTs embedded in AAO templates with 25 nm inner core diameter and wall thickness of 5 nm were incorporated by depositing different metal contact electrodes on both sides of the template using E-beam evaporation technique. The samples were covered with a shadow mask of circular holes made from an aluminum foil sample resulting in an active device area of 0.07 cm^2.

3.2 Characterization Procedures

Characterization procedures form the core of this research work. They not only helped to extensively study the properties of Carbon Nanotubes fabricated but also helped in establishing the cause of failures thereby allowing room for improvements in the processing steps. The devices and structures fabricated as a part of this thesis primarily relied on the following procedures for characterizations: Field Emission Scanning Electron Microscopy, UV-Visual Absorption Spectroscopy, X-Ray Diffraction and I-V Analysis. The subsequent sections in this chapter attempt to present an encapsulated description of these procedures.

3.2.1 Field Emission Scanning Electron Microscopy

The scanning electron microscope (SEM) is a type of electron microscope that images the sample surface by scanning it with a high-energy beam of electrons in a raster scan pattern. The electrons interact with the atoms that make up the sample producing signals that contain information about the sample's surface topography, composition and other properties such as electrical conductivity.

The types of signals made by an SEM can include secondary electrons, back scattered electrons, characteristic x-rays and light (cathodoluminescence). These signals come from the beam of electrons striking the surface of the specimen and interacting with the sample at or near its surface. In its primary detection mode, secondary electron imaging, the SEM can produce very high-resolution images of a sample surface, revealing details about 1 to 5 nm in size. Due to the way these images are created, SEM micrographs have a very large depth of focus yielding a characteristic three-dimensional appearance useful for understanding the surface structure of a sample. This great depth of field and the wide range of magnifications (commonly from about 25 times to 250,000 times) are available in the most common imaging mode for specimens in the SEM. Characteristic x-rays are the second most common imaging mode for an SEM. X-rays are emitted when the electron beam removes an inner shell electron from the sample, causing a higher energy electron to fill the shell and give off energy. These characteristic x-rays are used to identify the elemental composition of the sample. Back-scattered electrons (BSE) that come from the sample may also be used to form an image. BSE images are often used in analytical SEM along with the spectra made from the characteristic x-rays as clues to the elemental composition of the sample.

A Hitachi Field Emission Scanning Electron Microscopes (Model S-900) with a maximum magnification power of 800kX was used for characterizing MWNTs embedded in AAO templates. A Hitachi Field Emission Scanning Electron Microscopes (Model S-4300) was used to characterize the CNT-polymer and CNT-nanocrystalline composites. To image a particular sample, a very small section of the sample was cut-off from the original sample and mounted on a double-sided sticky carbon tape stuck on a SEM stub. The sample was coated with colloidal graphite on the edges and a known thickness of Gold-Palladium alloy was sputter coated to ensure proper electrical conductivity throughout the sample Specimens were imaged for both topology as well as cross-sectional views. Imaging helped in ascertaining the pore diameters, inter-pore distances and amorphous carbon layer thicknesses. Imaging also helped in understanding the effect of polymers and nanocrystalline on the sensor response.

3.2.2 Transmission Electron Microscopy

Transmission electron microscopy (TEM) is a microscopy technique whereby a beam of electrons is transmitted through an ultra thin specimen, interacting with the specimen as it passes through it. An image is formed from the electrons transmitted through the specimen, magnified and focused by an objective lens and appears on an imaging screen, a fluorescent screen in most TEMs, plus a monitor, or on a layer of photographic film, or to be detected by a sensor such as a CCD camera. The contrast in a TEM image is not like the contrast in a light microscope image. A crystalline material interacts with the electron beam mostly by diffraction rather than absorption, although the intensity of the transmitted beam is still affected by the volume and density of the material through which it passes. The intensity of the diffraction depends on the orientation of the planes of atoms in a crystal relative to the electron beam; at certain angles the electron beam is diffracted strongly from the axis of the incoming beam, while at other angles the beam is largely transmitted. Modern TEMs are often equipped with specimen holders that allow the user to tilt the specimen to a range of angles in order to obtain specific diffraction conditions, and apertures placed below the specimen allow the user to select electrons diffracted in a particular direction. A high-contrast image can therefore be formed by blocking electrons deflected away from the optical axis of the microscope by placing the aperture to allow only unscattered electrons through. This produces a variation in the electron intensity that reveals information on the crystal structure, and can be viewed on a fluorescent screen, or recorded on photographic film or captured electronically.

This technique (known as Bright Field or Light Field) is particularly sensitive to extended crystal lattice defects in an otherwise ordered crystal, such as dislocations. As the local distortion of the crystal around the defect changes the angle of the crystal plane, the intensity of the scattering will vary around the defect. As the image is formed by the distortion of the crystal planes around the defect, the contrast in these images does not normally coincide exactly with the defect, but is slightly to one side. It is also possible to produce an image from electrons deflected by a particular crystal plane. By either moving the aperture to the position of the deflected electrons, or tilting the electron beam so that the deflected electrons pass through the centered aperture, an image can be formed of only deflected electrons, known as a Dark Field image.In the most powerful diffraction contrast TEM instruments, crystal structure can also be investigated by High Resolution Transmission Electron Microscopy (HRTEM), also known as phase contrast imaging as the images are formed due to differences in phase of electron waves scattered through a thin specimen. A JEOL 2010FX transmission electron microscope with Ultra High Resolution Pole Piece was used to characterize the Carbon Nanotubes for examining their crystallinity and multi walled structure.

3.2.3 X-Ray Diffraction of the sample

X-Ray Diffraction is a non-destructive characterization technique widely employed to ascertain the elemental composition and crystal structure of a particular material under investigation. The diffraction pattern gives the phase, structure and different components of material examined. When an X-ray beam hits the atoms of the material, the electrons oscillate in different directions giving some constructive and destructive interference depending on the arrangement of atoms. The diffraction of X-rays in different h, k, l planes causes the reflections and the interplanar spacing d among the planes gives the intensities of the peaks at the detector angle 2-THETA. The diffraction pattern is a plot of reflected intensities versus 2-THETA or THETA. The corresponding 2-THETA value for the peak depends on the anode material of the X-ray tube. The d-spacing and 2-THETA satisfy Bragg's law given by

$$2d\sin\theta = n\lambda$$

Where n is an integer, λ is the wavelength of the X-rays.

Every known material existing in elemental, alloy in compound form has an X-Ray spectrum associated with it which is characteristic of that particular material. Thus, X-Ray diffraction is typically used to ascertain the quality (or degree of purity) of a particular substance. For the purpose of this thesis work, X-Ray diffraction spectra were used to infer the quality of anodized porous alumina templates and the Carbon Nanotubes grown in the pores as well as grown on Silicon substrates.

A Bruker-AXS D8 DISCOVER Diffractometer was used to obtain the X-ray diffraction spectra of all the films deposited. The template\substrate was first properly aligned w.r.t. to the X-ray source and the detector. After alignment, automated proprietary software was used to obtain the diffraction spectrum for 2θ values from 3^0 to 90^0 of angles of incidence. Patterns thus obtained were cross-referenced with the spectra in the reference database for suitable match and identification of compounds present in the sample.

3.2.4 **UV-Vis Absorption Spectroscopy**

Absorption spectroscopy in the optical and ultraviolet wavelengths is a routine procedure employed in chemistry to quantitatively determine solutions of transition metal ions and conjugate organic compounds. Optical absorption spectroscopy is a method used to obtain the band gap energy of the material examined. When the sample is hit with photons, the electrons on the surface of the sample absorb the photons having energy greater than that of the band gap energy and jump to the conduction band. However, the wavelength vs. absorption spectra that is obtained by the means of a UV-Vis spectrophotometer can also be used to infer the band-gap energy of crystalline films using Tauc's Law. The Carbon Nanotubes were obtained by dissolving the porous alumina matrix in 50% Phosphoric acid. The UV-Vis spectroscopy was used to infer the optical properties of the Carbon Nanotubes suspended in 50% Phosphoric acid medium. Absorption spectrum of a material being studied is usually obtained against a specific background, in this case the spectrum obtained from 50% Phosphoric acid.

The experimental procedure involved using a Cary-50 v3.0 UV-Visual Spectrophotometer to scan 50% Phosphoric acid first as the background; the other with CNTs suspended in acid medium was then subsequently scanned and was plotted after the subtracting the background. Samples were typically scanned in between wavelengths of 200 nm to 1100 nm. A detailed explanation of the graphs hence obtained is summarized in the next chapter.

3.2.5 Electrical Characterization of CNT arrays

Current–voltage measurements were the backbone for the characterization procedures performed on Aligned Carbon Nanotube devices. Besides giving an idea of how the currents flowing through the device change as a function of the voltage applied, the current-voltage plots were also employed to collect other valuable information about a device namely, the Carbon Nanotube Resistance (R_{CNT}), Contact resistance (R_{CON}) and Carbon Nanotube Resistivity (ρ_{CNT}). The effect of various metal contacts (Al, Ag, Ti, Cu, Au, Ni, Au/Pd, Pt) on the current-voltage (*I-V*) characteristics has been thoroughly investigated.

For studying the transport mechanism, metal contacts of area $0.07 cm^2$ were deposited under high vacuum by e-beam evaporation technique on both sides of the template. These devices were characterized for their electrical properties by Current–Voltage (I–V) measurements at room temperature as shown in figure 3.5.

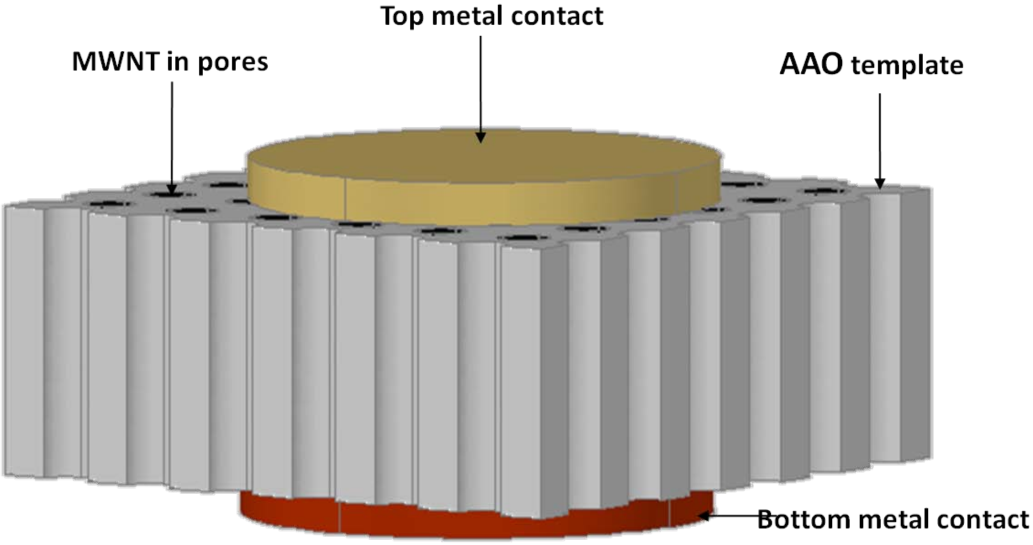

Fig 3.5 Schematic of MWNT based devices for transport mechanism studies.

It was found that a Schottky barrier was formed between the metal contact and the MWNTs at room temperature and plays a significant role in the transport through vertically aligned CNT arrays.

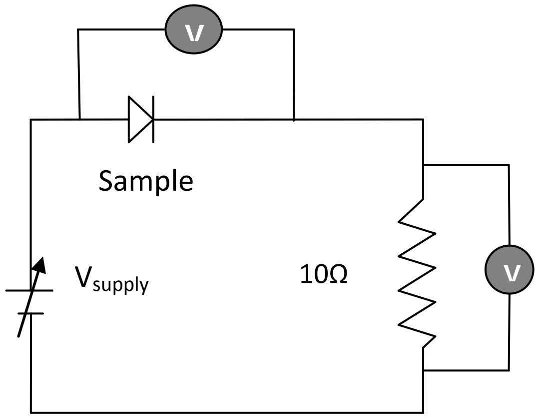

Fig 3.6 Block diagram of I-V measurement system

The experimental procedure to obtain the current vs. voltage plot at room temperature involved the use of a solar simulator equipped with a Kepco programmable bipolar operational amplifier/power supply (Model BOP 36-12M) and two Keithley digital multimeters employed as voltmeters (Model 2001 and 2000) interfaced with a common lab PC using an application software (LabVIEW Student Edition 7.0) provided by National Instruments. Supply voltages were varied from -4 Volts to +4 Volts in steps of 0.1 Volts. Corresponding values of current were measured and logged in the form of .txt files.

The number of MWNTs involved in conduction, required for the calculation of the R_{CNT} and ρ_{CNT} was obtained by calculating the area of the sample, which in turn was obtained from a stylus Profilometer measurement. The area of sample was confirmed by optical microscope measurements in the clean room.

3.3 Sensor Measurement Procedure

MWCNT based devices integrated into resistive sensor design by depositing contact electrodes were evaluated for their sensor response by measuring the change in resistance across the two bus bars when exposed to alternate cycles of Analyte (Test Gas) and Nitrogen.. A HP 3478A digital multimeter, interfaced with Lab View software, was employed to measure the change in resistance upon exposure to analyte gases. All experiments were carried out at room temperature while, the sensor was placed inside a sealed glass test chamber and the change in the device resistance was monitored as the chamber was cycled between analyte gases and nitrogen.

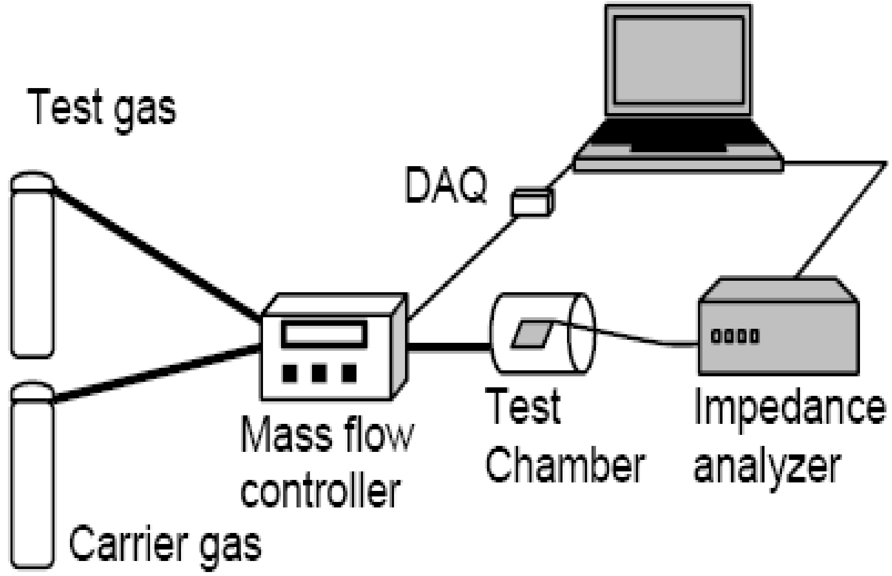

Fig 3.7 Schematic of the setup for Gas Sensing experiments

A Sierra Instruments dual channel mass flow controller was employed to control the flow rates of the purging gases and was controlled by LABVIEW interface through a National Instruments USB-6009 Data Acquisition device (DAQ). Nitrogen (N_2) was used as the carrier gas in all experiments and the test gases used included NH_3 and NO_2. Prior to the injection of test gas, the sensor chamber was flushed with nitrogen gas for at least 20 minutes. Using the mass flow controllers, the test gas was then injected and the percentage change in resistance (% $\Delta R/R$) of the device was monitored continuously for every 10 min alternate injections of test gas and the carrier gas.

4 Results and Discussion

4.1 Characterization of CNT based devices using Scanning Electron Microscopy

4.1.1 Characterization of AAO templates

To date, the most regular arrays of pores with the most uniform dimensions rely on repetitive anodization/etch cycles. During the first anodization step, an aluminum oxide surface, which is rough and covered with disordered pores, is generated as shown in figure 4.1(a). By removing the oxide layer with a wet chemical etch solution, a patterned aluminum surface is revealed. as shown in figure 4.1(b). The aluminum surface acts during a second anodization step as a template for the formation of highly ordered pores of aluminum oxide as shown in figure 4.1(c).

Scanning electron microscopic observations revealed that the porous AAO templates fabricated by the method described in section 3.1.1 were free standing membranes open ended on both sides. The pore diameter for templates anodized at 40V was 35 nm as shown in 4.1(c). Geometrically, the pores are approximately hexagonal in shape. The pores homogeneously cover the entire anodized region. It was observed that the pores formed as a result of anodization were increasingly well-ordered as the film grows thicker[82], hence an aluminum tape with an optimum thickness of 60µm was used to anodize long enough to achieve good pore–pore long-range order (that is, regions with the same hexagonal order), especially during the first step of anodization. It was observed that the surface of the aluminum changes in the course of anodization. The texturing of the aluminum is why the second anodization was believed to lead to a more ordered array of pores, because the surface of the aluminum has been textured from the array of ordered pores leaving the surface.

From the pore variation studies, it was observed that the pore diameter was primarily a function of the applied potential, typically in the range of 1.0–1.2 nm V^{-1}. For the sample shown in Fig. 4.1(c), anodized at 40Volts in 0.3M Oxalic Acid solution for more than 20 hours, long range uniformity of pores and the high porosity of the surface (1012 pores cm−2) was observed.

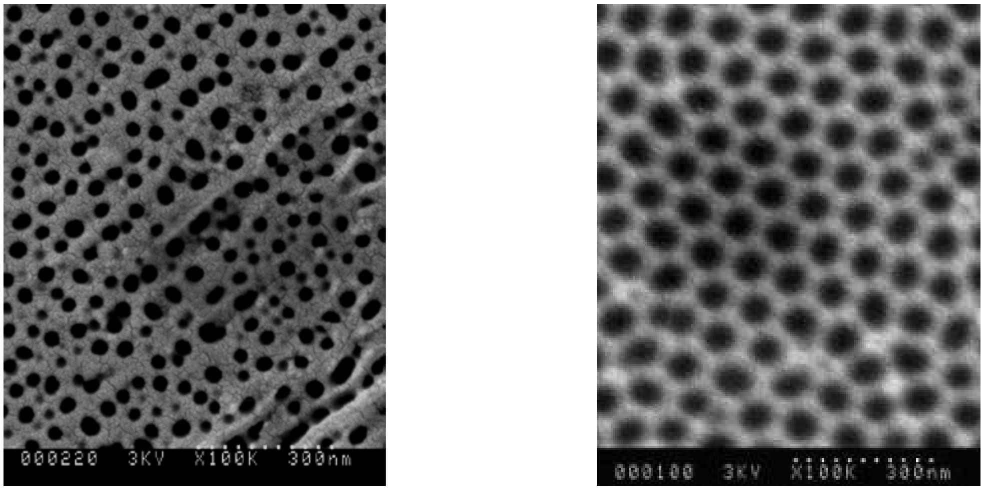

(a) (b)

Figure4.1: (a) SEM of Aluminum tape after first step anodization at 40V for 20 minutes; (b) SEM of after two step anodization at 40V for 22 hours.

The effect of various anodization voltages on the pore diameter and inter pore spacing were carefully investigated by using 10% vol. H_2SO_4 and 10% vol. H_3PO_4 acid bath solutions respectively.

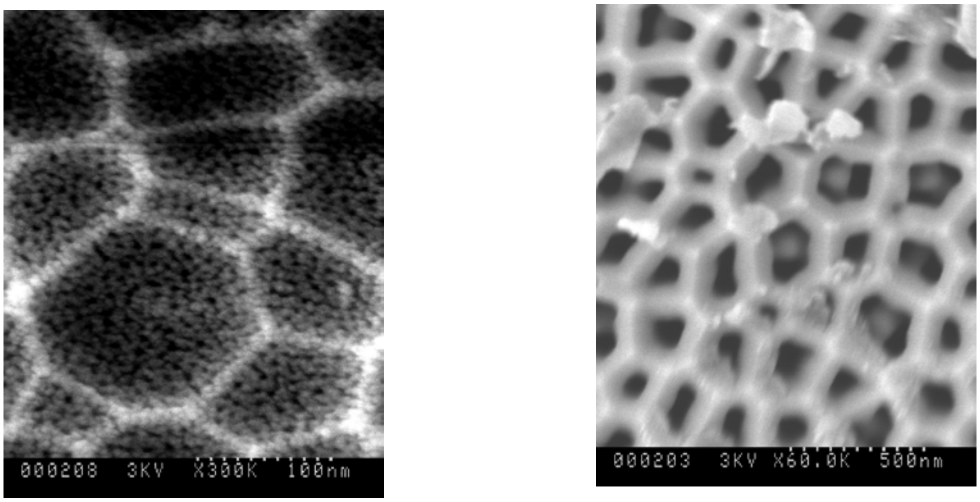

(a) (b)

Figure4.2: (a) SEM of Aluminum tape anodized at 5V in 10% vol. H_2SO_4; (b) SEM of Aluminum tape anodized at 10V in 10% vol. H_2SO_4.

Figure 4.2(a) shows a micrograph of the sample anodized in 10% vol. H_2SO_4 at 5V in 5^0C ambient temperature. The pores formed were very small with the pore diameter in the range of 8-10 nm. The surface is rough and the geometry of the pores was also not uniform. Figure 4.2(b) shows

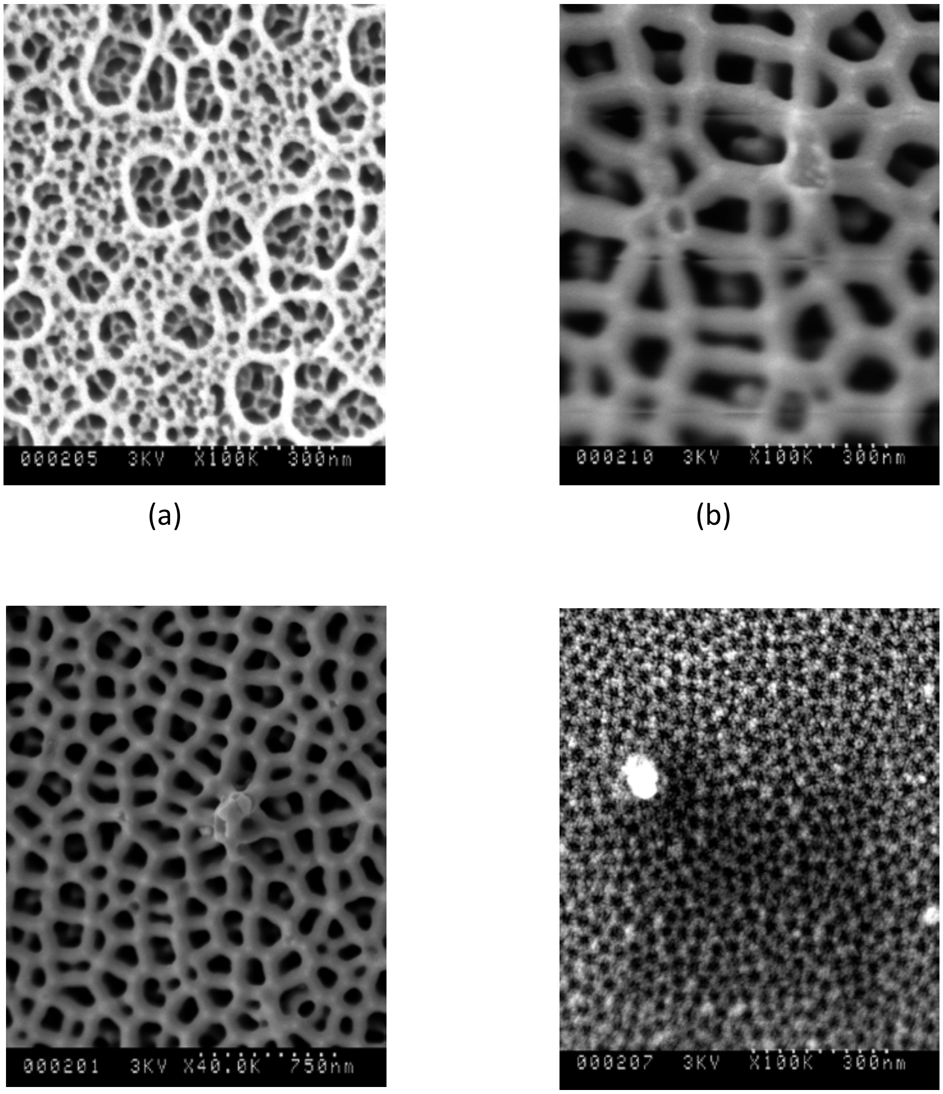

(a) (b)

(c) (d)

Figure4.3: (a) SEM of Aluminum tape anodized at 20V in 10% vol. H_3PO_4; (b) SEM of Aluminum tape anodized at 60V in 10% vol. H_3PO_4; (c) SEM of Aluminum tape anodized at 80V in 10% vol. H_3PO_4; (d) SEM of Aluminum tape anodized at 120V in 10% vol. H_3PO_4;

The aluminum oxide walls were thicker in the case of Al tape anodized in 10% vol. H_3PO_4 at 60V resulting in larger inter-pore distances in comparison with the case of the Al tape anodized at 40V as shown in Fig. 4.3(b). The uniformity of pores was observed to be increasing with increase in anodization voltages. On the other hand, wall thickness was decreasing with increasing voltages. Figure 4.3: (a) shows a micrograph of the sample anodized in 10% vol. H_3PO_4 at 20V in 5^0C temperature. The surface is rough and the geometry of the pores was also not uniform. Figure 4.3(d) shows. Highly aligned pores with high pore density were observed in templates anodized in 10% vol. H_3PO_4 at 120V. The pore diameter was in the range of 27-30nm.

4.1.2 Characterization of CNTs grown in AAO Templates

Multi Walled Carbon nanotubes grown in the pores of highly ordered porous alumina templates without the use of a catalyst by CVD process were characterized by Scanning Electron Microscope technique. It was observed that the CNT\AAO templates were free standing with open ended nanotubes on both top and bottom surfaces as shown in Fig. 4.4(a). To further corroborate this observation, a mild phosphoric etch was performed to etch the aluminum oxide on both sides thereby, nanotubes protruding from the top and bottom surfaces of the template were observed as shown in Figs. 4.4(b).and 4.4(c) respectively. A thin layer of amorphous carbon (a-C) was formed as a bi-product of the CVD process on both sides of the template which plays a key role in the sensor response. The thickness of the amorphous carbon can be varied between 5nm and 40nm by either tailoring the CVD growth process conditions or by post growth processing. The temperature and the time of reaction determine the thickness of the a-C layer during the CVD growth process while, its thickness can be varied by different plasma oxidation techniques as part of post growth processing. Fig. 4.5(a) shows a CNT/AAO template with thicker amorphous carbon layer (~40nm) while Fig. 4.5(b) shows a template with thinner a-C layer (~5 nm). The thickness of a-C layer in this device was tailored during the CVD growth process. Fig. 4.5(c) shows a device where the a-C layer was completely removed by oxygen plasma oxidation technique and tubes protruding from the top and bottom surfaces were observed.

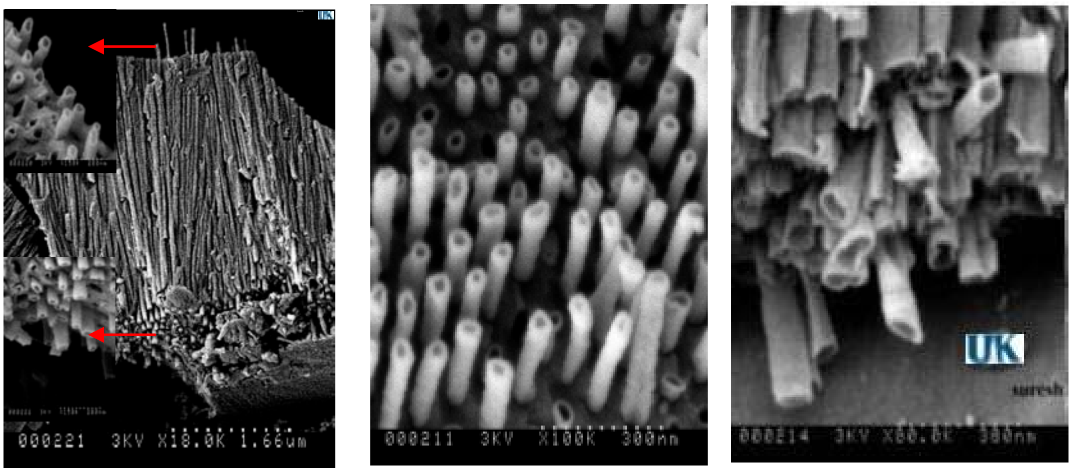

(a) (b) (c)

Figure4.4: (a) Cross sectional image of a CNT/AAO template, inset showing top and bottom open ends. (b) Tubes protruding from the top surface after phosphoric acid etch; (c) Tubes protruding from the bottom surface after phosphoric acid etch.

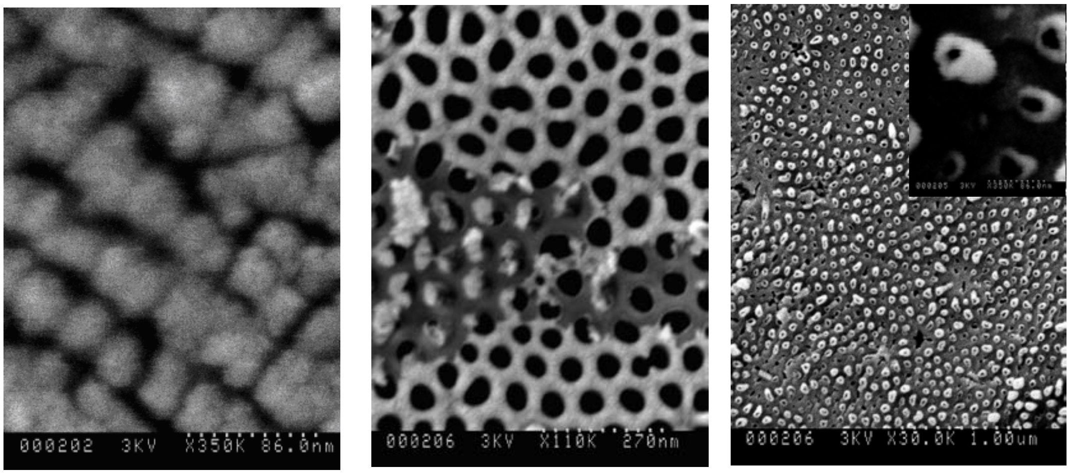

(a) (b) (c)

Figure4.5: (a) MWCNTs in AAO with thick amorphous carbon top layer; (b) MWCNTs in AAO with thin amorphous carbon top layer; (c) MWCNTs in AAO with amorphous carbon layer removed.

All of the CNTs grown in our study were Multiwalled in nature. This is understandable because alumina itself is acting a catalyst strong enough for the decomposition of xylene and plays a critical role in the formation of MWCNTs in the AAO template. The AAO pore walls also acts as a guide for the vertical growth of the nanotubes. At this point, it is important to note the Lewis acid nature of surface sites in amorphous and transition alumina plays an important role in their intrinsic catalytic activity in the decomposition or recombination of unsaturated hydrocarbons [83]. Assuming that the internal alumina walls have uniform catalytic properties, then the xylene pyrolysis may occur with the same probability at any point on the wall. Under this assumption, the internal pore walls will be covered by carbon flakes, resulting in the formation of multiwall carbon nanotube (MWNT) structures [84].

4.1.3. Characterization of CNTs grown on Silicon substrates

Thick films of multi walled carbon nanotubes grown on Si/SiO_2 substrates by CVD process using a Ferrocene catalyst were characterized by Scanning Electron Microscope. These observations revealed that thick films of MWNTs with uniform diameters were formed on these substrates with a thin layer of amorphous carbon deposited on the top as a bi-product of the CVD process as shown in Fig. 4.6(a). The thin amorphous carbon layer was removed by plasma oxidation technique as shown in Fig. 4.6(b) and it was observed that the nanotubes were of uniform diameter with their length spanning from 80 - 90 µm depending on the CVD growth conditions.

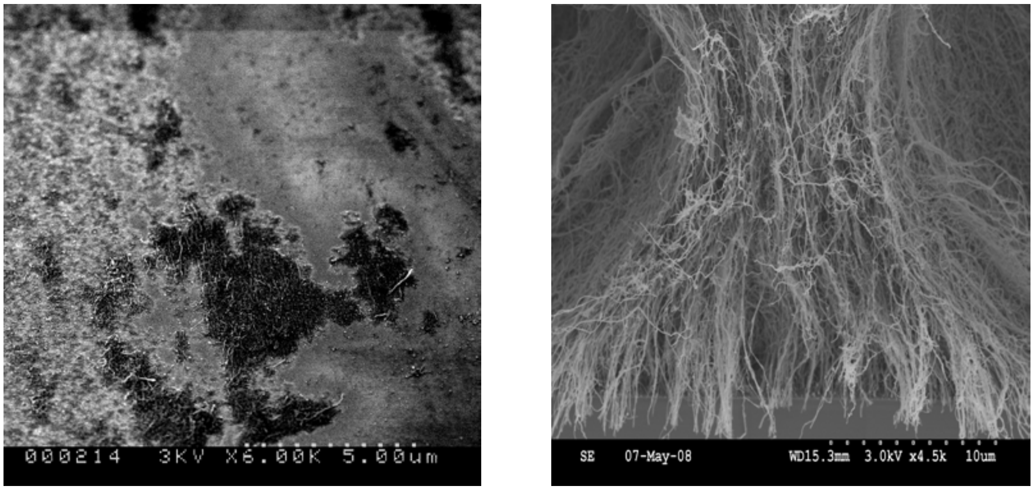

(a) (b)

Figure4.6: (a) Thick films of Multi walled carbon nanotubes grown on Si/SiO_2 substrates with amorphous carbon layer on the top surface; (b) Cross sectional SEM micrograph of a thick film of Multi walled carbon nanotubes grown on Si/SiO_2 substrates.

4.1.4. Characterization of CNT-polymer composites

Thick films of Multi walled carbon nanotubes grown on Si/SiO_2 substrates were spin coated with a PEDOT: PSS polymer layer to enhance the sensor response. Fig 4.7(a) shows the bundles of MWNTs with the PEDOT: PSS spin coated while Fig 4.7(b) shows a higher magnification image of the polymer spin coated device. The thin layer of amorphous carbon layer formed as the bi-product of the CVD growth process was removed by plasma oxidation technique, prior to the spin coating of the polymer. It was observed that the polymer increased the connectivity between the as grown nanotubes which is in agreement with the sensors results explained in the later sections.

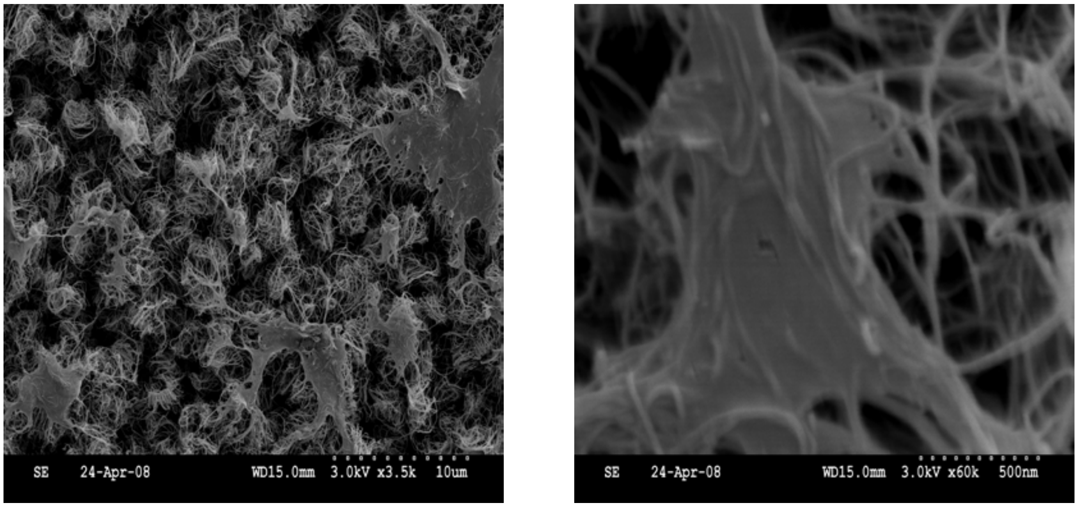

(a) (b)

Figure4.7: (a) Thick films of Multi walled carbon nanotubes grown on Si/SiO_2 substrates spin coated with PEDOT: PSS polymer; (b) Magnified SEM micrograph of Multi walled carbon nanotubes grown on Si/SiO_2 substrates spin coated with PEDOT: PSS polymer.

4.1.5. Characterization of CNT- nanocrystalline composites

Hybrid nano composite MWNT sensors were fabricated by spin coating 0.01 Molar TiO_2 sol gel solution on thick films of multi walled carbon nanotubes grown on Si/SiO2 substrates. These nano-composite sensors were characterized by using SEM and it was observed that the Titania nano crystalline particles adhere to the walls of individual nano tubes as shown in Fig. 4.8(b).

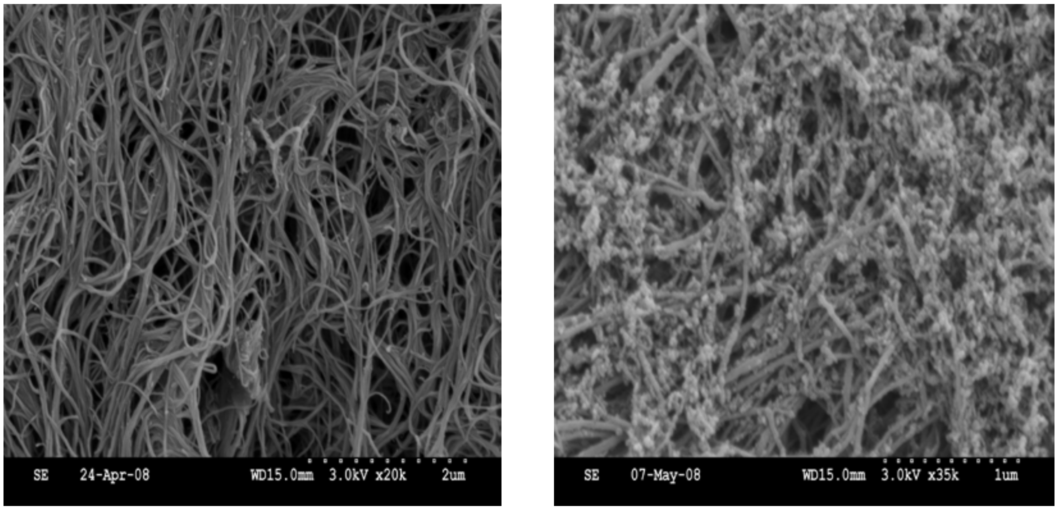

(a) (b)

Figure 4.8: (a) Network of Multi walled carbon nanotubes grown on Si/SiO_2 substrates; (b) Network of Multi walled carbon nanotubes grown on Si/SiO_2 substrates after spin coating 0.01M TiO_2 solgel solution; Titania nano crystalline particles can be seen around each nanotube.

4.2 Characterization of CNTs using Transmission Electron Microscopy

The carbon nanotubes spanned the entire length of the template with open ends on both sides, as shown in Fig. 4.4(a). Next, the alumina template was dissolved in phosphoric acid to release the tubes for TEM measurements. Transmission electron microscopy confirmed that the tubes were open ended and the walls are crystalline. The outer diameter of the free-standing nanotubes was 40 nm which was the AAO pore diameter in the case of the Aluminum tape anodized at 40 V. The wall thickness of the nanotube was 5 nm on either side making the inner diameter 30 nm as shown in Fig. 4.9(a). From the TEM observations, the distance between two neighboring fringes was about 3.4 Å, in agreement with the inter-planar separation of graphite (3.35 Å). Also, TEM observations revealed that the tube walls were smooth with homogeneous thickness. The growth of Carbon nanotubes appears to be initiated by the walls of the alumina template, where alumina itself is acting as a catalyst.

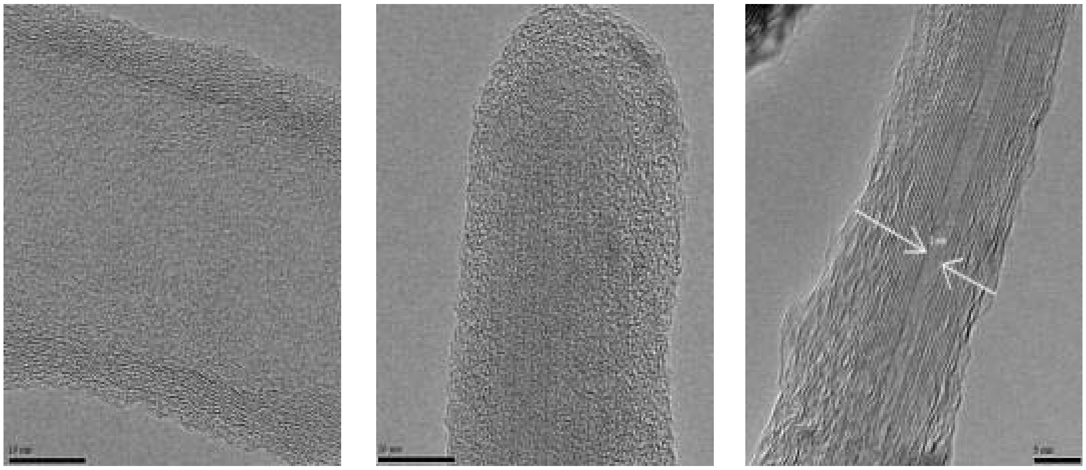

(a) (b) (c)

Figure 4.9: (a) Transmission electron micrograph of the Multi walled Carbon nanotube grown in AAO template; distance between two neighboring fringes (walls) is about 3.4Å; (b) TEM of the 2nm MWNT showing a closed end; (c) TEM of the MWNT with 2nm core diameter.

In case of the CNTs grown in the AAO template with a diameter of 12 nm, the TEM analysis showed Multiwalled carbon nanotubes with crystalline walls and a core diameter of 2 nm as shown in Figure 4.9(c). It is interesting to note that the smallest diameter CNTs obtained in the present study (2 nm) were close ended as shown in figure 4.9(b), while all larger diameter CNTs were open ended. This close ended nature of the smallest diameter (2nm) CNT arrays as a hindrance, since the ends can be opened through post processing by either chemical or dry etch process. Hence, these membranes are potential candidates for nanoscale filtration. They can also serve as tools for fundamental studies of mass transport in confined environments [13].

4.3 Characterization of CNTs using X-Ray Diffraction

The X-ray diffraction pattern obtained for a plain anodized alumina template annealed in oxygen at 700° C for 5 hours is shown in Figure 4.10. The 2-THETA values at which the peaks were obtained (44.4° and 64.845°), show that the free standing porous alumina templates fabricated by anodization technique and annealed at 700° C for 5 hours were of the form γ- Al_2O_3 [85]. Annealing at 700° C for 5 hours in oxygen environment aided in improving the crystallanity and purity of the Aluminum oxide.

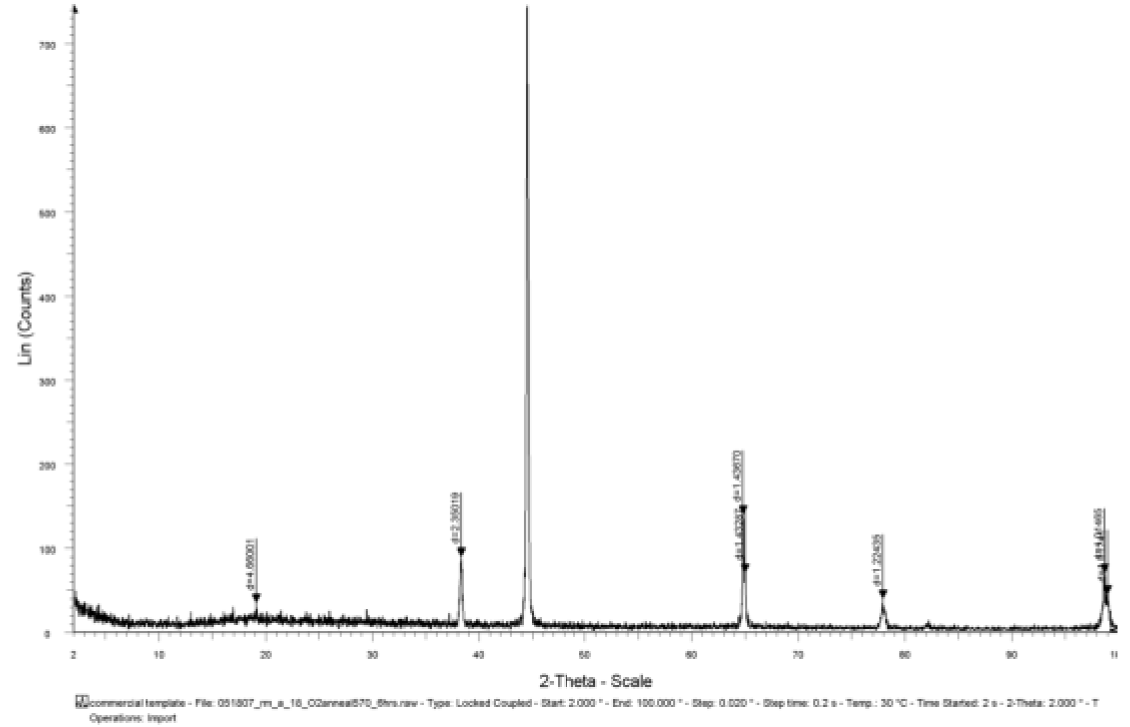

Figure 4.10: X-Ray Diffraction pattern of an AAO template annealed in oxygen at 700^0 C for 6 hours.

Caption	Angle (2-Theta °)	d value(Angstrom)	Intensity(count)	Intensity%
d=4.66001	19.029	4.66001	34.0	4.6
d=2.35019	38.266	2.35019	89.0	11.9
d=2.03494	44.486	2.03494	746	100.0
d=1.43670	64.845	1.43670	139	18.6
d=1.43287	65.040	1.43287	70.0	9.4
d=1.22435	77.975	1.22435	39.0	5.2
d=1.01465	98.783	1.01465	70.0	9.4
d=1.01241	99.080	1.01241	44.0	5.9

Table 4.1 X-Ray diffraction parameters for an AAO template annealed in oxygen at 700^0 C for 6 hours.

4.4 Characterization of CNTs using UV-Vis Absorption Spectroscopy

Figure 4.14 is the UV-Vis absorbance spectra of MWCNTs suspended in aqueous medium as described in section 3.2.4. The peak absorbance of CNT suspension was observed at 252nm which corresponds to CNT absorbance peak [86,87]. The absorbance depends on the amount of nano particles in the nanofluid. In addition, other secondary parameters such as particle size, shape, dispersion, stability, etc. are also the keys in determining the absorption behavior. Higher exposed surface area of CNTs is another reason for higher absorbance in CNT suspension. The Beer–Lambert law expresses a linear relationship between an absorbance of light and the properties of a material through which light is passing. The law can be expressed in the following way:

$$A = \alpha l c$$

A is the absorbance, α the absorption coefficient (L in mol−1 cm−1), l (cm) the distance that light travel through material and c is the concentration (mol L−1) of absorbing species in the material. This law is applicable to measure the absorbance of light in nanofluid [88-90]. Chemical and instrumental factors that limit the linearity of the Beer–

Lambert law are generally very high concentrations and its electrostatic interaction at close proximity, shift in equilibrium as a function of concentration and fluorescence of the sample, etc. Due to polarity of the treated CNTs, electrostatic interactions between CNTs exist in their suspension.

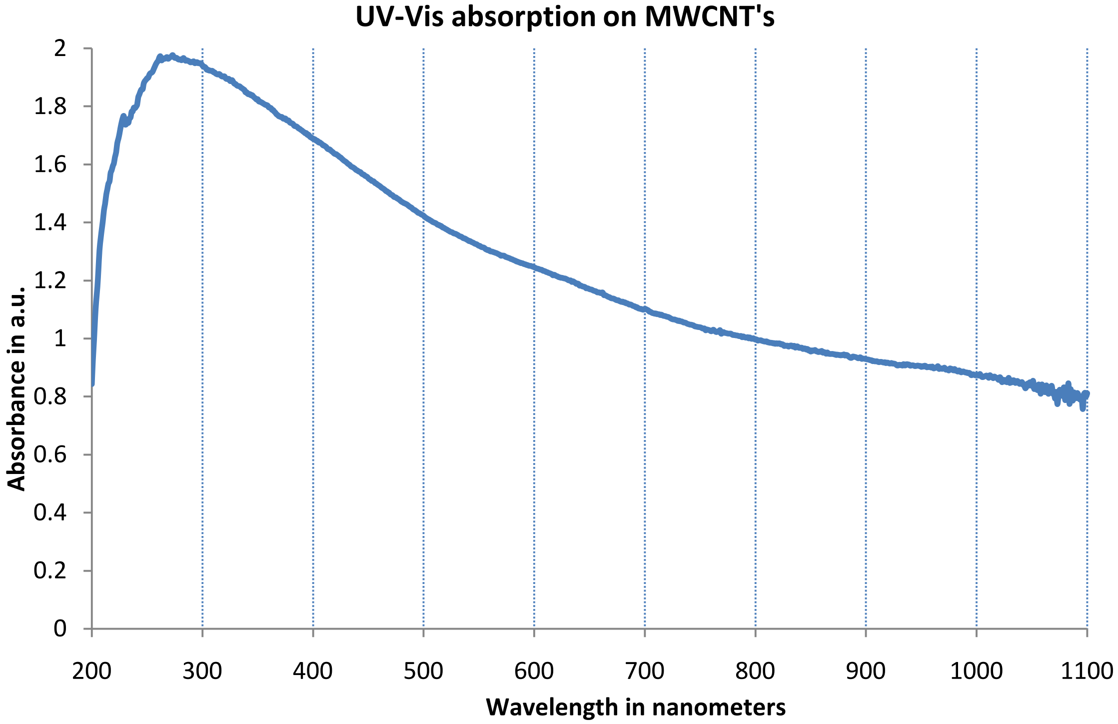

Figure 4.11: UV-Vis absorbance spectra of MWCNTs suspended in aqueous medium.

4.5 Electrical Characterization of CNT arrays

For studying the transport mechanism properties in aligned multi walled carbon nanotubes, metal contacts of area 0.07cm^2 and 100nm thick were deposited on both sides of the template as described in section 3.1.7. Post metallization annealing was also done at 200^{o}C to reduce the effects of contact resistance. These devices were characterized for their electrical properties by Current–Voltage (I–V) measurements at room temperature.

The number of CNTs involved in current transport under each metal dot were calculated from the pore density which in turn was calculated from a high magnification SEM image; typical pore density was 180-200 pores/ μm^2 for a standard AAO template anodized at 40V in Oxalic acid medium at 4^oC.

A typical I-V curve with an ohmic behavior was observed for a device with platinum electrodes deposited on both sides, as shown in figure 4.15. This current-voltage characteristic yielded a value of resistivity for multiwall carbon nanotubes embedded in an AAO array. The value of resistivity was in the range of 100-150 Ω-cm which was reproducible on several devices.

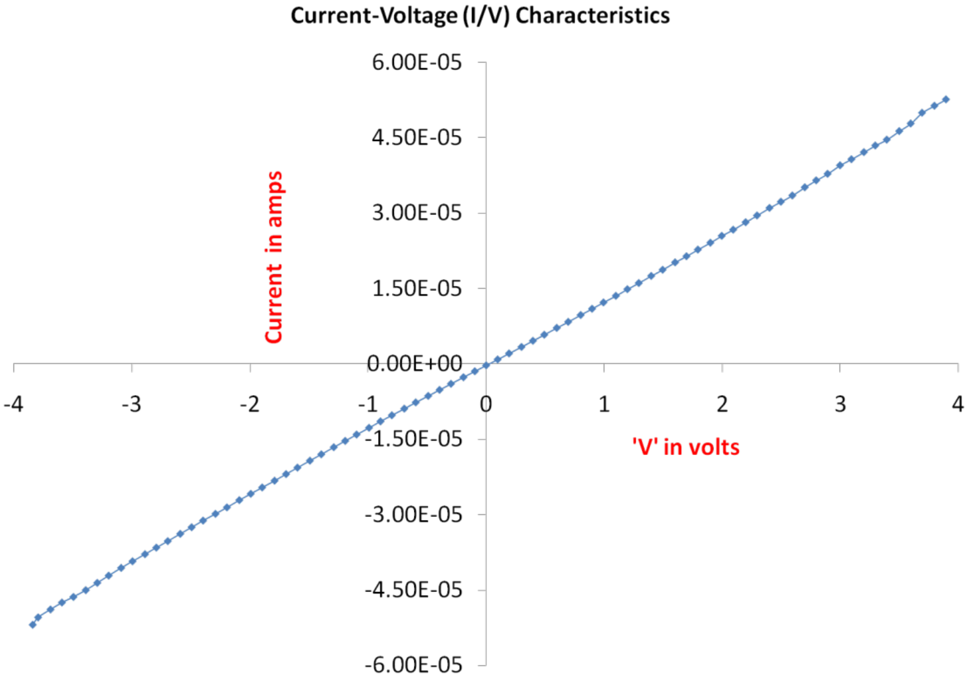

Figure 4.12: Current-Voltage characteristics of a vertically aligned Multiwalled carbon nanotube device with platinum electrodes deposited on both sides.

Sample calculation for the resistivity of a vertically aligned multi walled carbon nanotube is as follows:

Sample ρ_{CNT} Calculation

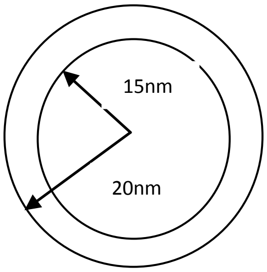

Area of the sample = 0.0936 cm^2

Pore density = 120-140 pores / μm^2

Pore diameter = 40nm, inner core diameter = 30nm

Length of CNTs' = 60 µm. = 60E-04 cm

Area of the ring = π [$(20nm)^2$- $(15nm)^2$] m^2

= 549.5E-14 cm^2

Assuming the pore density to be 130E+08 pores / cm^2

We get the number of CNTs' = (Area of sample) x (Pore density)

= 7.9625E+08

Area of CNTs' in contact to the metal = (no. of CNTs') x (Area of one CNT ring)

= 4.37541E-03 cm^2

Average resistance from room temperature I-V characteristics = 705.21596 Ω

Contact resistance from high temperature I-V characteristics = 555.11162 Ω

Therefore, R_{avg} = 151.104341 Ω

ρ_{CNT} = (R_{avg})(Area of CNTs' in contact to the metal)/length of CNTs').

= 110.190537 Ω-cm.

Figure 4.13 shows I – V characteristics from a MWCNT device with copper and platinum as top and bottom contact electrodes respectively. This asymmetrical I-V behavior of the CNTs observed at room temperature can be attributed to the presence of a Schottky barrier at the Cu/CNT interface. This can also be attributed to better crystallinity of our nanotubes grown through a template assisted method.

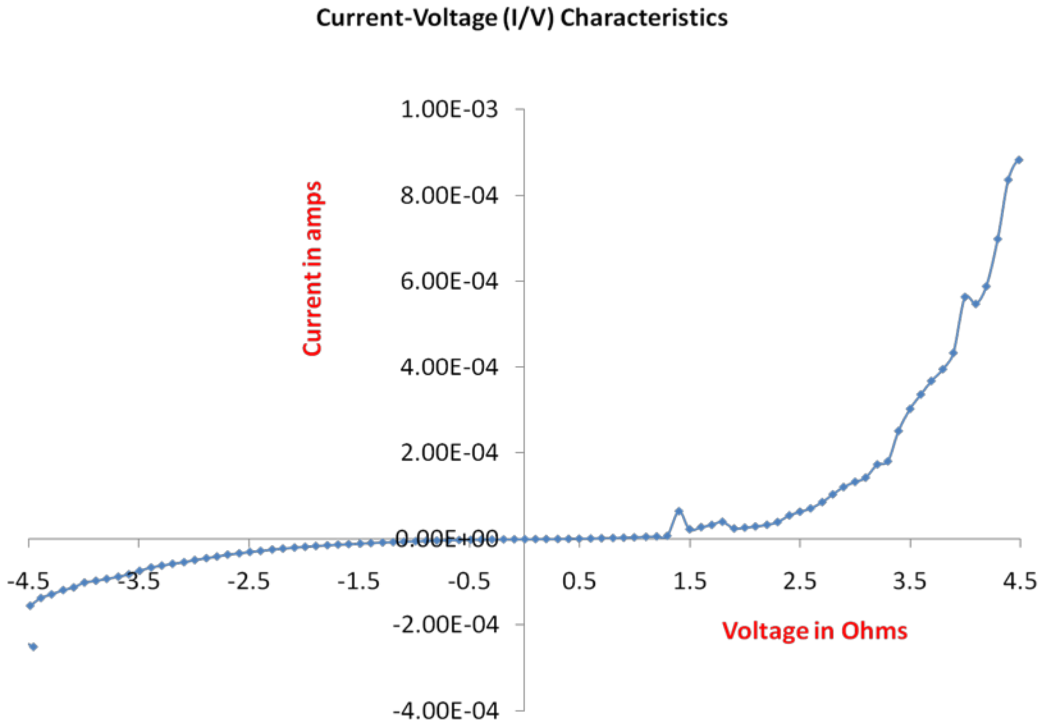

Figure 4.13: Current-Voltage characteristics of a vertically aligned Multiwalled carbon nanotube device with platinum and copper electrodes deposited on top and bottom sides of the template.

These observations, nanotubes forming ohmic contacts with higher work function metals (Au, Pt) and rectifying (Schottky) contact with lower work function metals (Cu, Al), implies that the multiwalled CNTs grown inside an insulating alumina matrix exhibit p-type semiconducting behavior. This also corroborates the results obtained from gas sensing experiments performed on these CNT devices where the resistance of the device increased when exposed to a reducing agent and decreased in the presence of an oxidizing agent.

4.6 Sensor Results

4.6.1 Sensor response of CNTs embedded in AAO

The MWCNT based sensor devices fabricated as discussed in section 3.1.3 were characterized for their sensor response. These sensors were highly responsive to both reducing gases like NH_3 and oxidizing gases like NO_2. The sensor response was evaluated by measuring the resistance upon exposure to various gases. The sensitivity (S) is defined as,

$$S(\%) = \frac{R_{gas} - R_{N_2}}{R_{N_2}} \times 100 \quad (1)$$

Where R_{N2} is the device resistance in the presence of carrier gas N_2, and Rgas is the resistance in the presence of test gas.

Figure 4.15 shows the sensor response of MWCNT/AAO device, when exposed to 0.01% NH_3. A sensor response of 10.5% for the first pulse, 4.3% in steady state and 14.9% cumulative was observed.

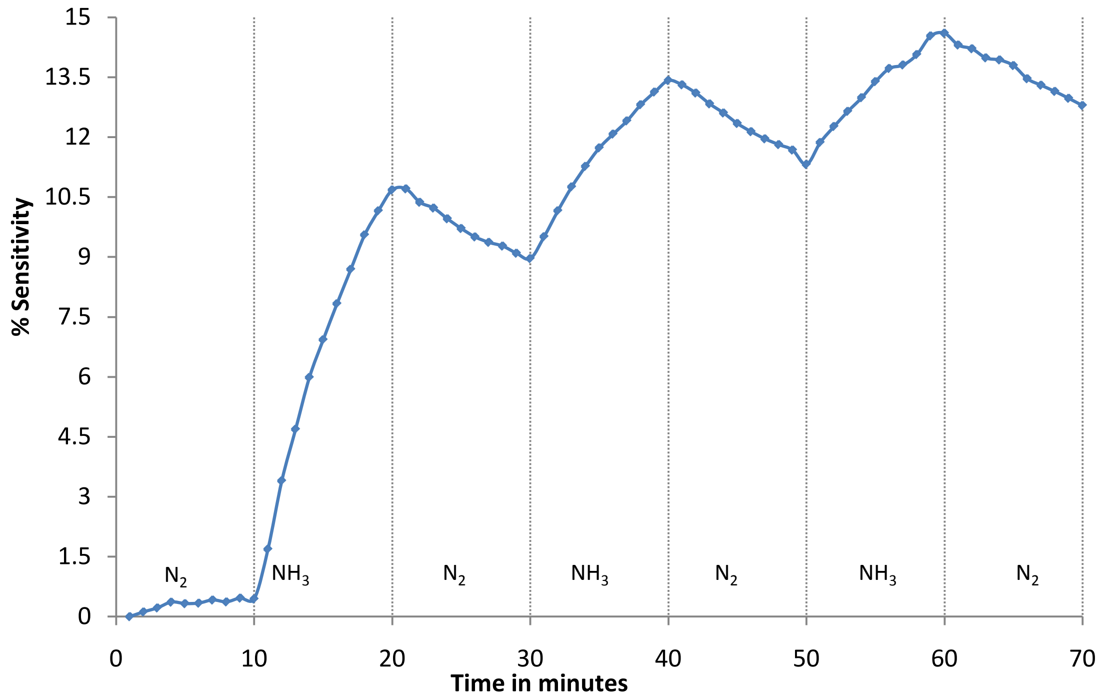

Figure 4.14: Response of MWCNT/AAO resistive sensor at room temperature to 0.01% NH_3

These sensor devices were also highly responsive to oxidizing agents like NO_2. Figure 4.15 shows the sensitivity of a MWCNT/AAO device exposed to 0.01% of NO_2 gas. sensor response of 33.62% for the first pulse, 12% in steady state and 49.3% cumulative was observed.

Alternate cycles of test gas and Nitrogen were purged and the corresponding values of resistance were noted and the sensitivity was calculated using the formula described earlier. The sensitivities obtained are higher than those reported earlier. The reason may be attributed to the adsorption of the gas molecules on the inner walls of the carbon nanotubes. The gas molecules are also believed to be adsorbed between the walls of the multi walled carbon nanotubes. The higher sensitivities are also due to the high surface area available for the gas molecules to be adsorbed. The well defined, highly ordered pores contribute to the high surface area of the MWCNT/AAO based sensor devices.

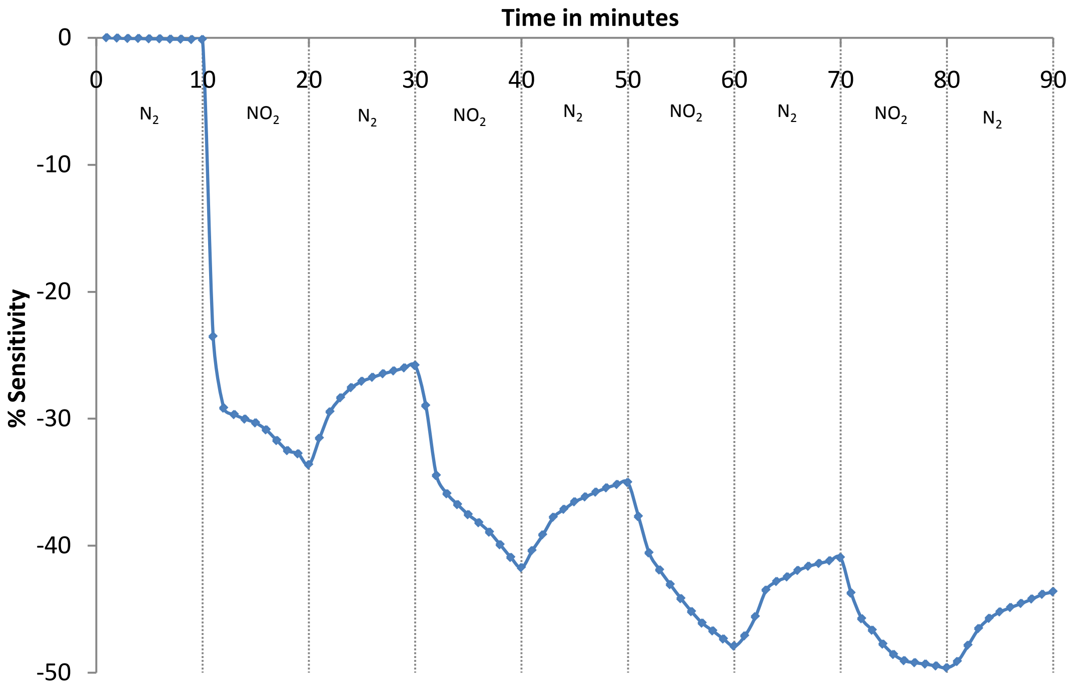

Figure 4.15: Response of MWCNT/AAO resistive sensor at room temperature to 0.01% NO_2

4.6.1.1 Effect of thickness of a-C layers on sensitivity

The amorphous carbon layer formed as the by-product of the Chemical Vapor Deposition process plays a crucial role in determining the sensitivity of the MWCNT/AAO based sensor device. The effect of amorphous carbon layer thickness on sensitivity of the device was investigated by varying the thickness of amorphous carbon (a-C) layers by both post growth processing as well as by tailoring the CVD growth conditions.

Initially, the dependence of the device sensitivity on the thickness of the a-C layer was studied by varying the CVD process growth conditions. Figures 4.16 and 4.17 compare the responses of thin and thick a-C layer devices exposed to NH_3, a reducing agent. For a device with thin a-C layers (5nm and 30nm on the top and bottom respectively), a baseline resistance of 0.3 MΩ and a sensor response of 12% for the first pulse, 5% at steady state, and 20% cumulative, were observed when exposed to 100 ppm of ammonia, as shown in Figure 4.17.

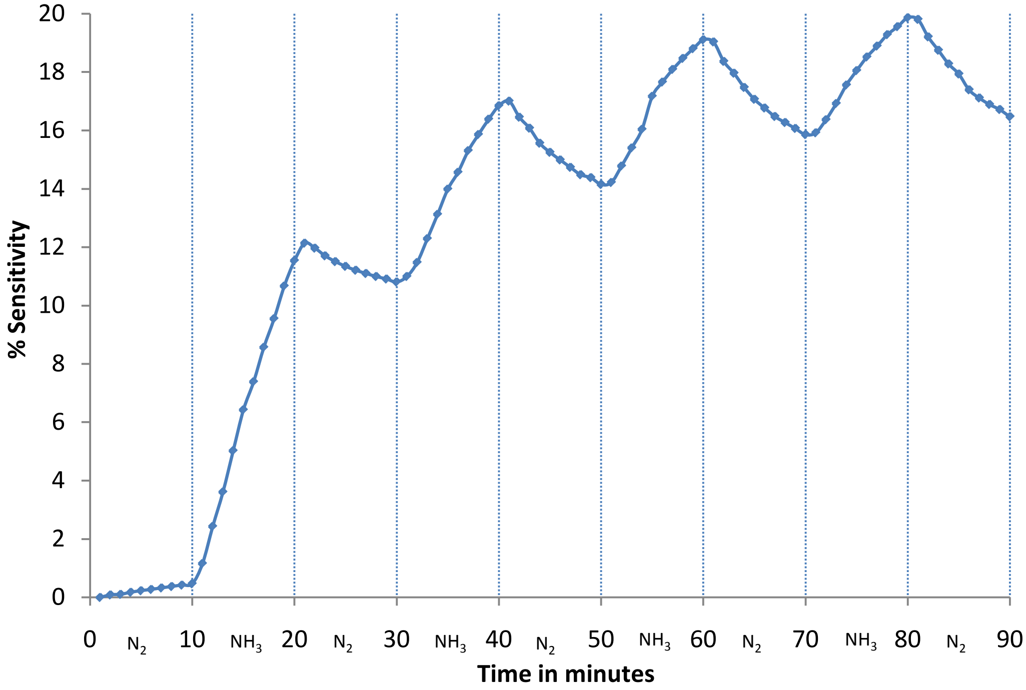

Figure 4.16: Response of CNT/AAO resistive sensor with thinner amorphous carbon at room temperature to 0.01% NH_3

Figure 4.17 shows the sensor response of thicker a-C layer device, when exposed to 1% and 5% NH_3. Sensor response to 5% NH_3 was observed to be 16% for the first pulse, and 9% in steady state. For 1% NH_3, responses of 6% for the first pulse and 5% in steady state were observed. The baseline resistance of thicker a-C layer devices was observed to be in the order of few hundred ohms which is significantly less when compared to thin a-C layer devices.

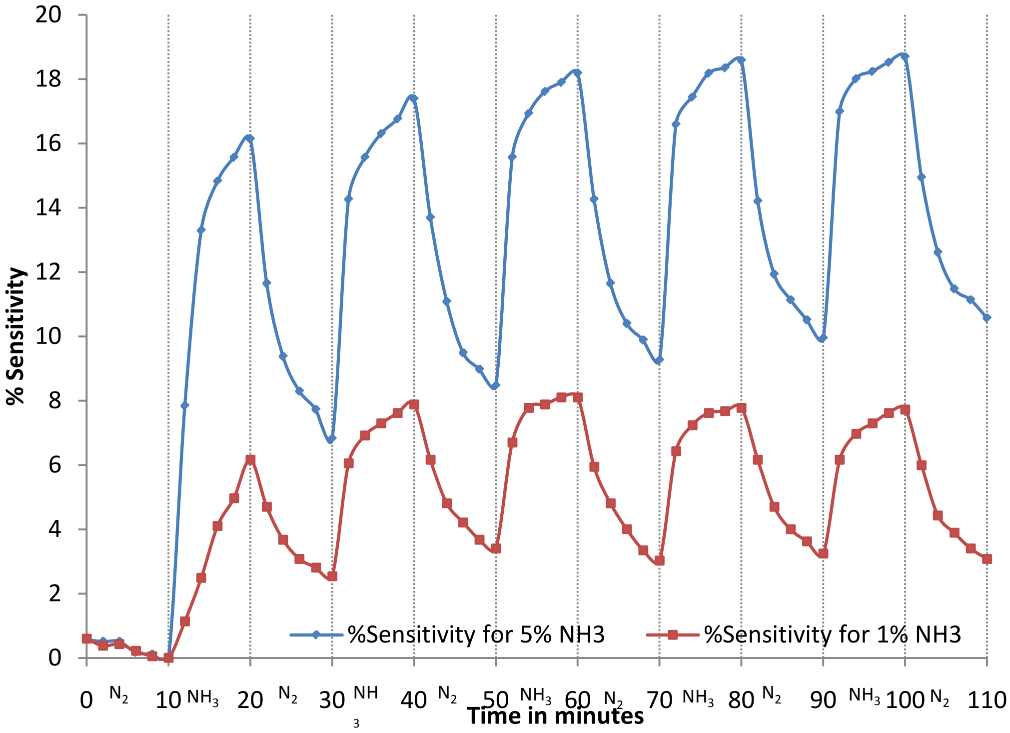

Figure 4.17: Response of CNT/AAO resistive sensor with thicker amorphous carbon at room temperature to 5% NH_3 and 1% NH_3

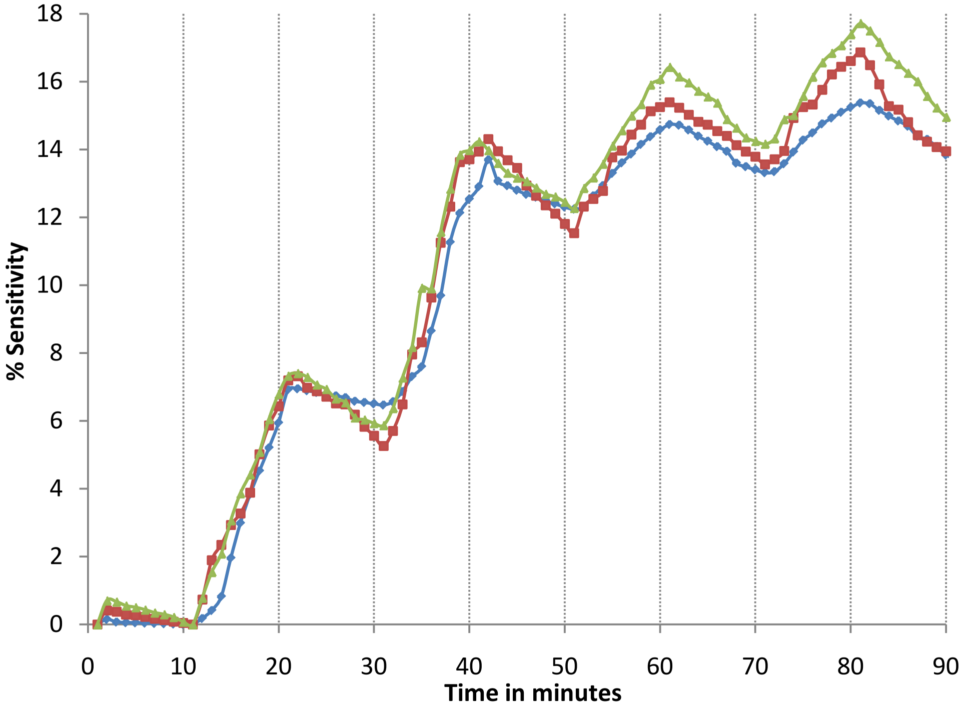

Figure 4.18: Response of MWCNT/AAO resistive sensor to 0.01% NH_3 with varying amorphous carbon layer thickness by post growth processing.

Thickness of the a-C layer was also varied by post growth processing by means of oxygen plasma oxidation as described in section 3.1.3. The sensor response of a MWCNT/AAO device to 0.01% NH_3 with various a-C layer thicknesses obtained by plasma oxidation technique is shown in Figure 4.18. The initial response (Blue) corresponds to as prepared sample with an a-C layer thickness of 40nm. The Baseline resistance was 2.78 Kilo ohms with 15.37% cumulative sensitivity. Then the sample was oxygen plasma oxidized for 30 sec to decrease the a-C layer thickness to 25nm and the corresponding sensor response (Red) is shown in Figure 4.18. The baseline resistance and the cumulative sensitivity were increased to 6.88Kilo Ohms and 16.86% respectively. The sample was further plasma oxidized for another 30 sec and evaluated for its sensor response to 0.01% NH_3. The sensor response (Green) is shown in figure 4.18. The baseline resistance increased to 9.27 kilo Ohms a cumulative sensitivity of 17.7% was observed. The increase in baseline resistance and device sensitivity with decreasing a-C layer thickness was found in agreement with the previous experimental results. These results underline the important role played by the amorphous carbon layer as a conducting contact between the adjacent CNTs, even though the primary sensing mechanism involves the interaction of the carbon nanotubes with the analyte.

4.6.1.2 Effect of UV light on Desorption

The electrical response of the resistive sensor indicates a charge transfer between the nanotubes and the gas molecules, and hence, the adsorption of gases on the inner walls of the nanotubes is the dominant sensing mechanism. As the sensor goes through NH_3 – N_2 cycles there is a buildup in chemisorbed NH_3 on the MWCNT surface, which causes an upward drift in the baseline resistance as well as the sensitivity. This is due to the fact that the adsorbate binding energy is sufficiently large and some of the ammonia molecules can be adsorbed at the defect sites available either on the nanotubes surface or on the inner walls of the open ended MWCNTs. The gas molecules adsorbed at these defect sites are hard to desorb. Hence, weakly bonded, physisorbed, molecules desorb with each cycle, while the more strongly bonded (chemisorbed or physisorbed at the defect sites) molecules remain during cycling. Binding energy is high enough that heat or ultraviolet light is needed to desorb the analyte and bring the MWCNTs back to its initial conducting state [10].

Experiments were carried out to study the effect of UV radiation on the recovery of the device baseline resistance by investigating desorption characteristics as shown in Figure 4.19. The sensor resistance fell steeply when UV light was used in combination with the carrier gas (N_2) during desorption cycle, which indicates that the strongly bonded analyte molecules can be completely desorbed by using high energy UV source, improving the desorption profile without any shift in the baseline resistance after the initial exposure. The recovery process is crucial for practical applications. Our recovery process is relatively simple which requires only the application of a relatively high energy UV light for a short period.

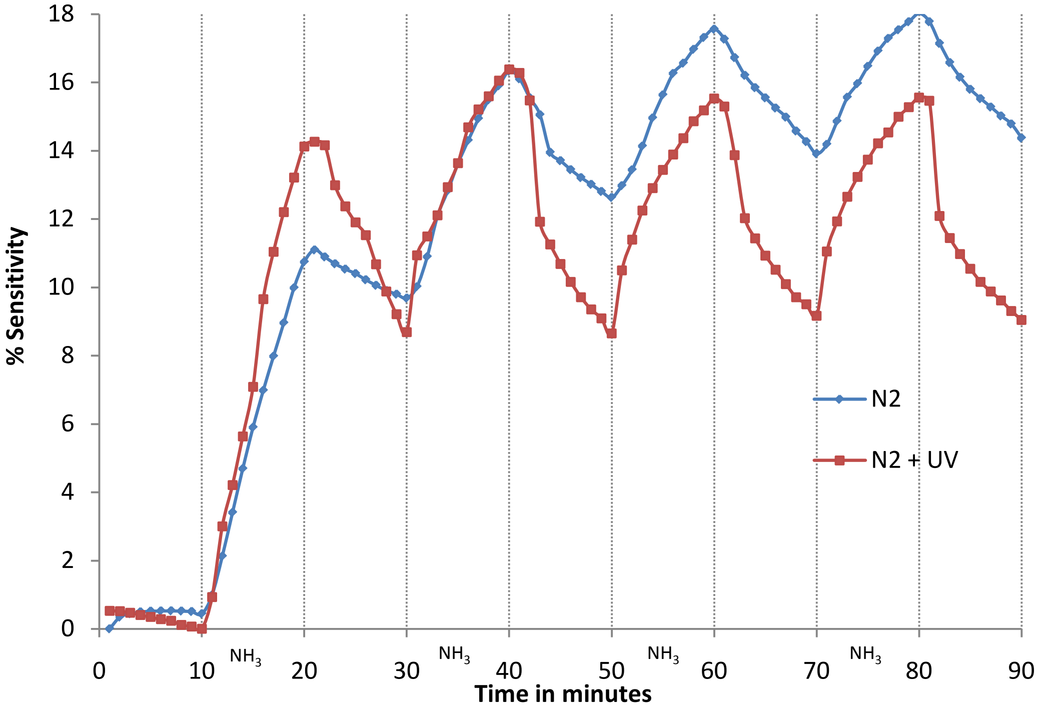

Figure 4.19: Response of CNT/AAO resistive to 0.01% NH_3 with different desorption techniques.

4.6.1.3 Effect of flow rate on Sensor response

A detailed study was conducted on the dependence of device sensitivity on flow rate of the test gas (NH_3) as shown in Figure 4.20. The sensitivity was found to increase with an increase in flow rate of the test gas up to 750 sccm and then decreased for 1000 sccm. The device sensitivity was highest for a flow rate of 750 sccm. The variation of device sensitivity with flow rate can be interpreted as follows. A change in device resistance occurs when the analyte gas species adsorb on the nanotubes. A flow of N_2 desorbs some species from the surface during N_2 cycles. Therefore, the flow rate is responsible for both the supply of species to the surface as well as desorption of the physisorbed species from the surface. Therefore when a sensor is exposed to an analyte gas (100 ppm NH_3 in N_2), both adsorption and desorption are taking place.

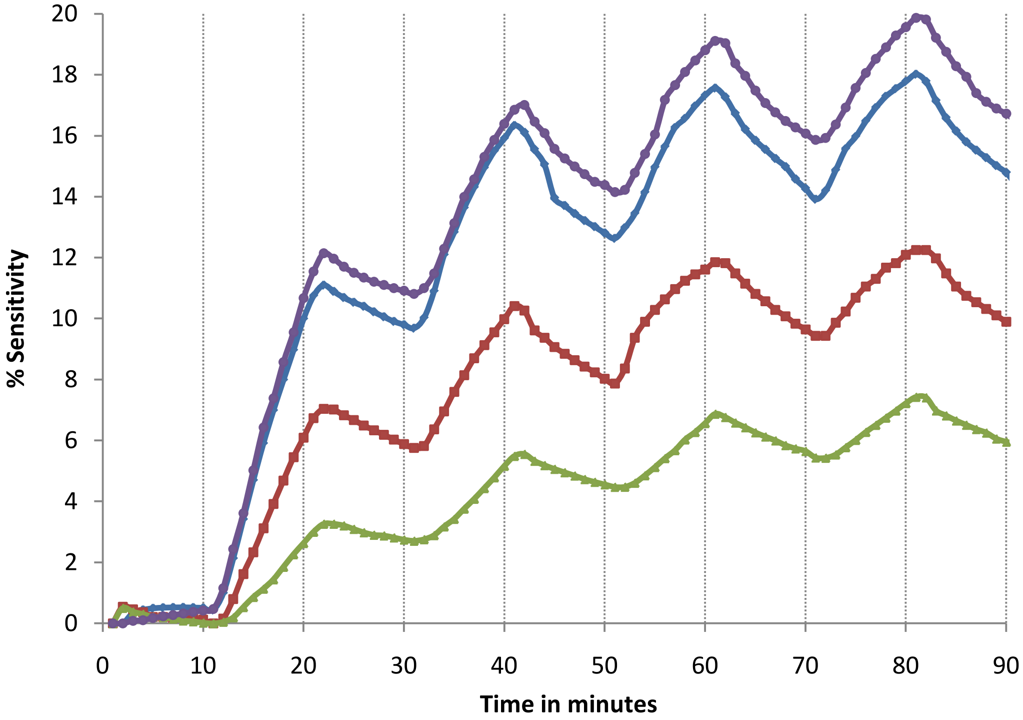

Figure 4.20: Sensor response of CNT/AAO resistive sensor to different flow rates of 0.01% NH_3

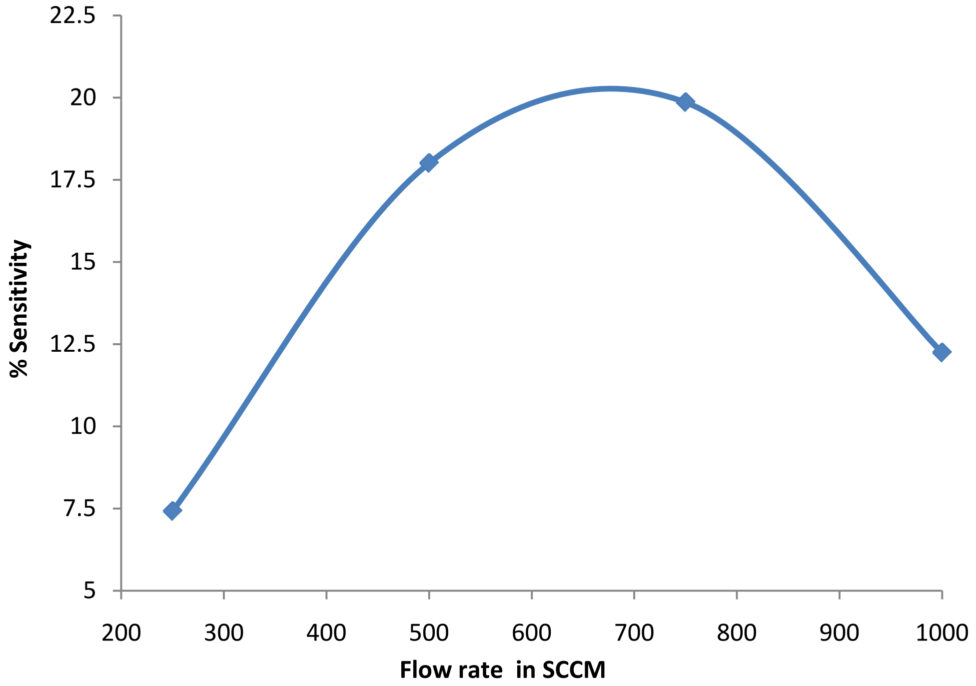

Figure 4.21: Sensitivity –vs – Flow rate of 0.01% NH_3 for a CNT/AAO resistive sensor.

Figure 4.21 shows a plot of flow rate vs sensitivity plot for a MWCNT/AAO sensor device when exposed to 0.01% of NH_3. The sensitivity increases as a function of flow rate up to 750 sccm. This can be understood as the mass transport limited regime, where an increased flow rate provides an increase of species to adsorb, resulting in an increased sensitivity. The increased flow of the analyte at higher flow rates (1000 sccm), promotes desorption, thus impacting the equilibrium concentration of adsorbed species even with an increase in the available species. The desorption characteristic of the flow-rate is important in understanding this behavior. If the gas flow didn't promote desorption, we would expect two regimes: mass transport limited and surface limited, with the latter showing no change in sensitivity with respect to flow rate.

4.6.2 Sensor response of CNTs grown on Silicon substrates

4.6.2.1 Response of as grown CNT-films

Free standing porous alumina templates integrated into resistive sensor design, with Multi walled Carbon nanotubes embedded in them were difficult to handle and had unique sensor characteristics. Thus CNTs grown as thick films on Silicon substrates as described in section 3.1.4 were integrated into resistive sensor designs which were robust in design and easy to handle. The as prepared film of MWCNTs on Si/SiO_2 substrates had a thin layer of amorphous carbon deposited due to which the sensor response of these devices was noisy as shown in figure 4.22. The response was improved by removing the layer of amorphous carbon by plasma oxidation technique. A sensor response of 2% for the first pulse and 2.6% cumulative, were observed for MWCNT film- resistive sensors to 0.01% NH_3 after 30 seconds plasma oxidation as shown in figure 4.23. The reason may be attributed to the conducting nature of the amorphous carbon between the two contact electrodes, without involving the thick film of MWCNTs underneath the a-C layer.

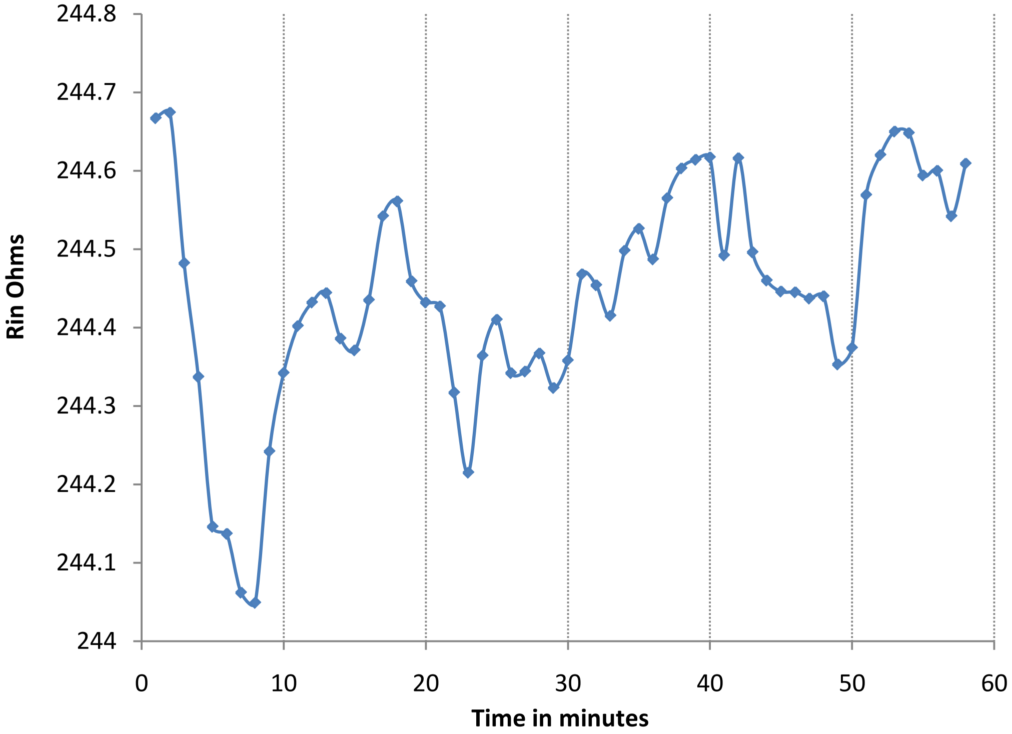

Figure 4.22: Response of as-grown MWCNT film resistive sensor to 0.01% NH_3 at room temperature.

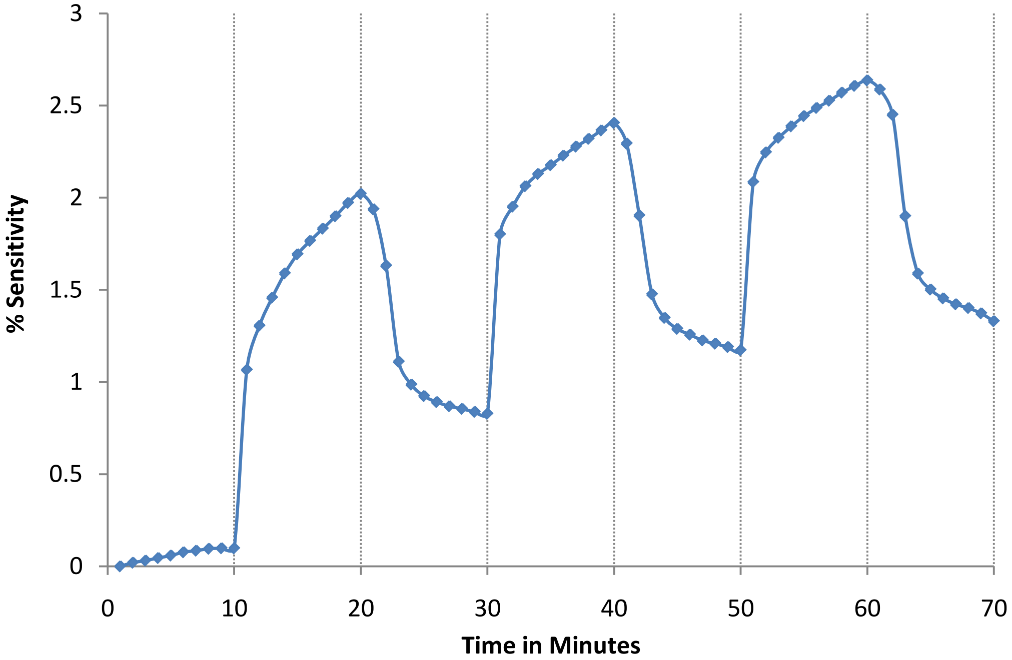

Figure 4.23: Response of MWCNT film resistive sensor to 0.01% NH_3 at room temperature after 30sec Plasma oxidation

Figure 4.24 shows sensor response of a MWCNT film to 0.01% NO_2 after 30sec Plasma oxidation. High sensitivities like 31% for the first pulse, 5% steady state and 32% cumulative were observed. These sensitivities are the highest ever reported sensitivities for as grown MWCNTs to very low concentrations of oxidizing gases like NO_2.

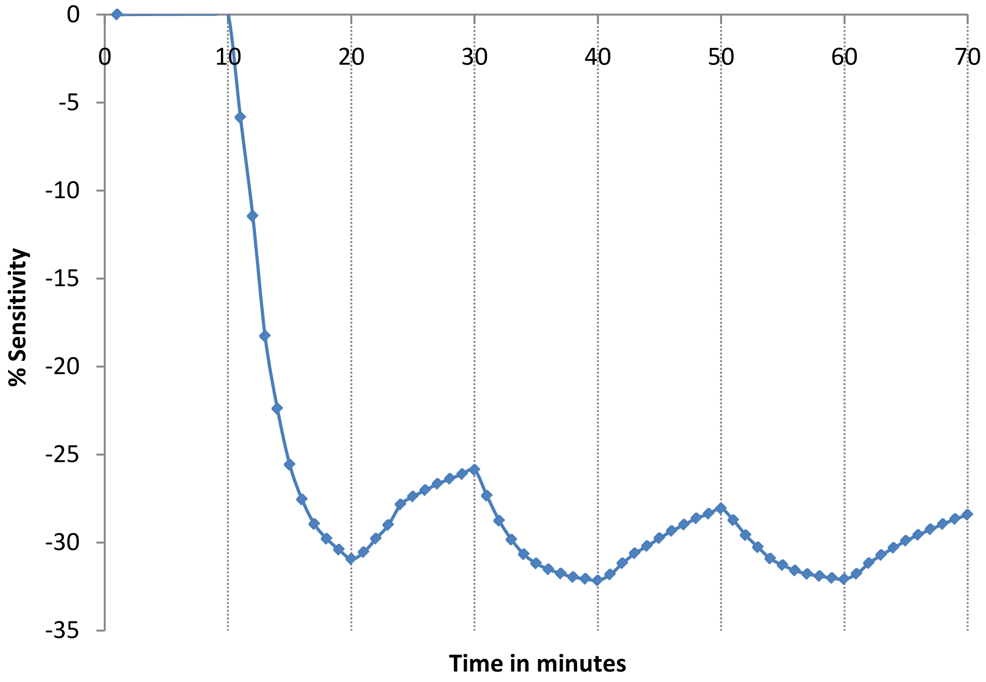

Figure 4.24: Response of a MWCNT film resistive sensor to 0.01% NO_2 at room temperature after 30sec Plasma oxidation

4.6.2.2 Response of CNT- polymer composites

PEDOT: PSS polymer is spin coated on oxygen plasma oxidized MWCNT film on Si/ SiO_2 substrates as described in section 3.1.5. These sensors were then evaluated for their sensor response to both oxidizing and reducing agents. Figure 4.26 shows the sensor response of PEDOT: PSS coated MWCNT film to 0.01% NH_3 at room temperature. A sensor response of 24% for the first pulse, 9% steady state and 23% cumulative was observed.

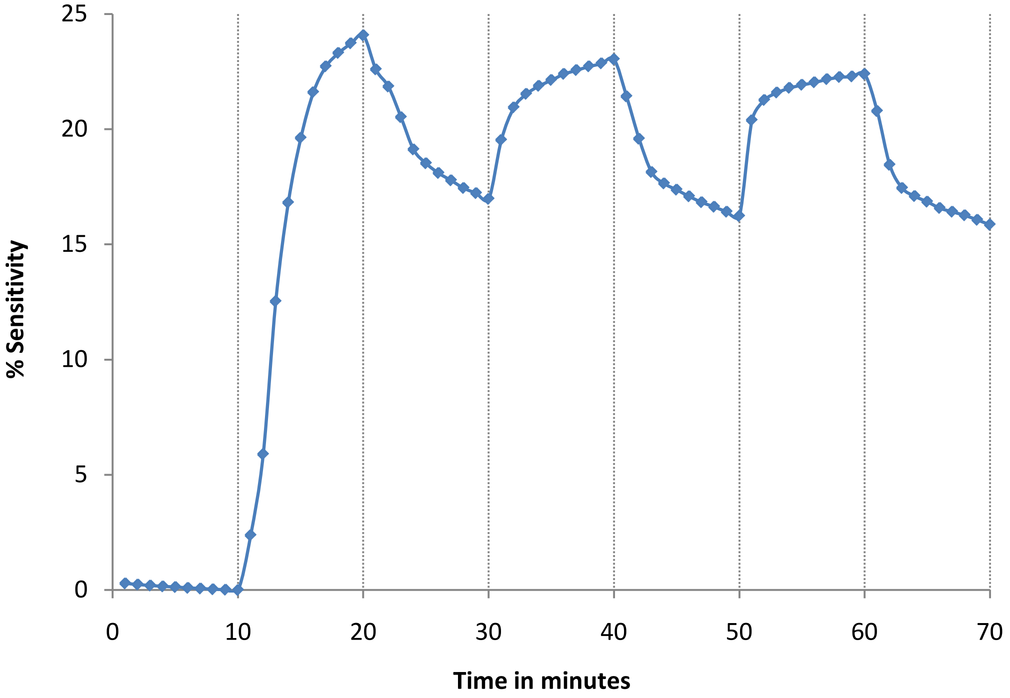

Figure 4.25: Response of a MWCNT film resistive sensor to 0.01% NH_3 after 30sec Oxygen Plasma oxidation and spin coating **PEDOT: PSS** polymer over the film.

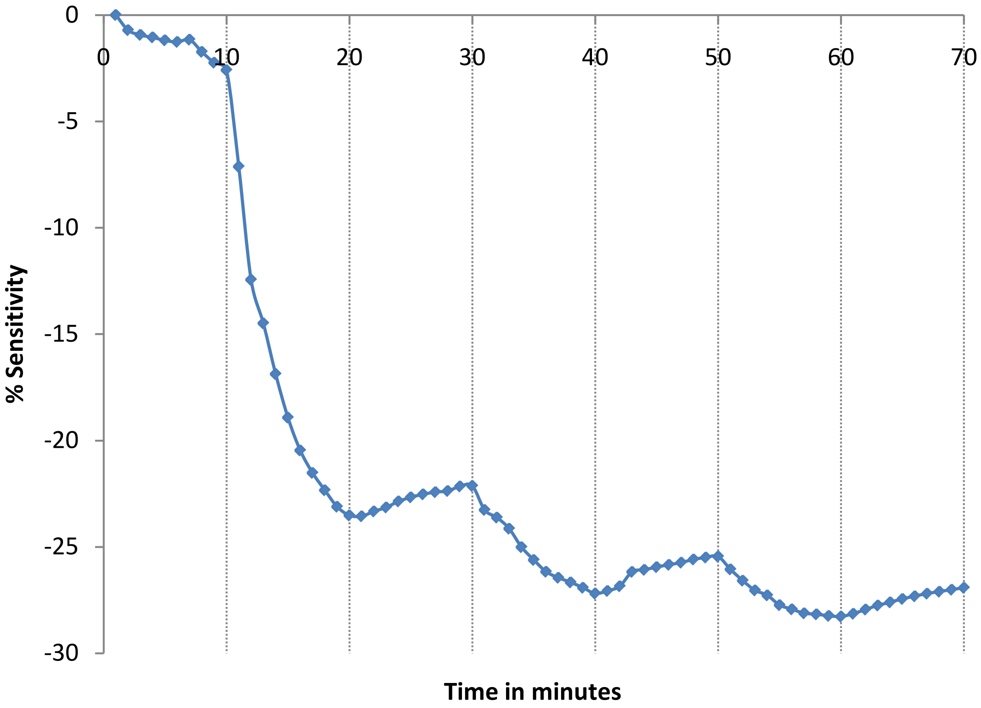

Figure 4.26: Response of a MWCNT film resistive sensor to 0.01% NO_2 after 30sec Oxygen Plasma oxidation and spin coating **PEDOT: PSS** polymer over the film.

The sensitivity was increased by an order of 10 when compared to as grown MWCNT film – resistive sensors. The reason may be attributed to the conducting nature of the polymer (PEDOT: PSS); providing a better conductive medium connecting the individual nanotubes grown as dense films. Thus a better signal transduction is achieved to the external measurement environment through the two deposited gold contact electrodes.

Similarly the device showed higher sensitivities to oxidizing agents like NO_2. Figure 4.27 shows the sensor response of PEDOT: PSS coated MWCNT film to 0.01% NH_3 at room temperature. A sensor response of 24% for the first pulse, 5% steady state and 29% cumulative was observed.

4.6.2.3 Response of CNT- Nanocrystalline composites

0.01M TiO_2 Solgel solution is spin coated on oxygen plasma oxidized MWCNT film on Si/ SiO_2 substrates as described in section 3.1.6. These sensors were then evaluated for their sensor response to both oxidizing and reducing agents. Figure 4.28 shows the sensor response of 0.01M TiO_2 solgel coated MWCNT film to 0.01% NH_3 at room temperature. A sensor response of 3.4785% for the first pulse, 1.54% steady state and 5.374% cumulative was observed.

Figure 4.29 shows the sensor response of 0.01M TiO_2 solgel coated MWCNT film to 0.01% NO_2 at room temperature. A sensor response of 18.54% for the first pulse, 3.24% steady state and 18.74% cumulative was observed.

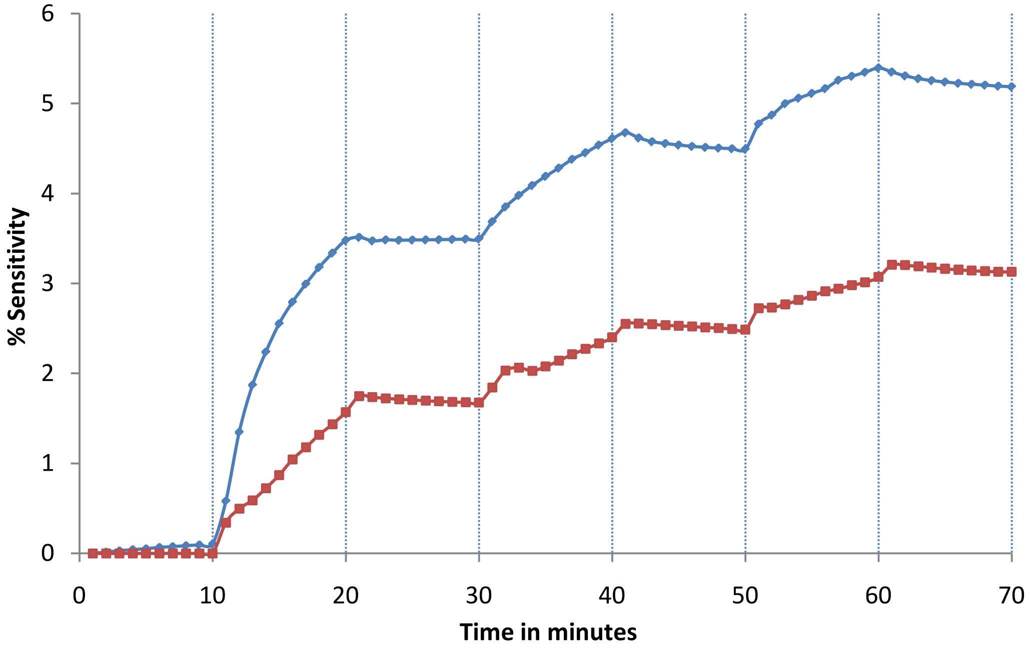

Figure 4.27: Response of MWCNT film- resistive sensor to 0.01% NH_3 ; (RED) after 30sec Oxygen Plasma oxidation; (BLUE) and spin coating 0.01M **TiO_2 nano crystalline solgel** solution over the film.

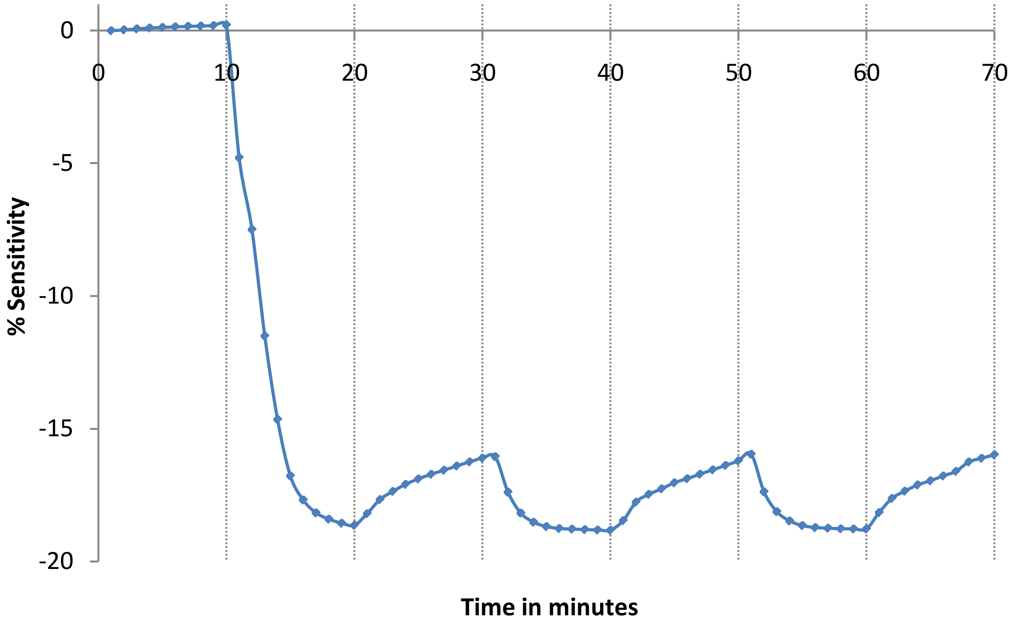

Figure 4.28: Response of MWCNT film- resistive sensor at room temperature to 0.01% NO_2 after 30sec Oxygen Plasma oxidation and spin coating 0.01M **TiO_2 nano crystalline solgel** solution over the film.

5. Conclusion and Scope for the future work

Highly ordered, vertically aligned carbon nanotubes (CNTs) were fabricated by xylene pyrolysis without the use of a catalyst inside an insulating alumina matrix. The post growth characterization by SEM and TEM showed that our nanotubes are well aligned, open ended on both sides with a wall thickness of 5 nm, and the walls are crystalline. These free standing nanoporous anodized aluminum oxide (AAO) membranes with MWCNTs in them were integrated into sensor designs for detecting NH_3 and NO_2 at room temperatures. The fabrication process of these resistive sensors is simple and does not require any special techniques like e-beam lithography nor photo-lithography. The sensors were responsive to both oxidizing and reducing species at room temperature and a detailed study was conducted on the dependence of sensitivity on the thickness of amorphous carbon layer on both top and bottom. The best response (12% for the first pulse, 5% steady state, and 20% cumulative change) was observed for a sensor with a thin amorphous carbon layer when exposed to 100ppm of ammonia. For sensors with thicker amorphous carbon layer, a 0.7% change for the first pulse and a steady state value of 0.6% change in resistance was observed when exposed to 100 ppm of NH_3.

The sensors also exhibited an excellent response (a cumulative response of 50% over 4 cycles, an initial response of 34% for the first pulse and a steady state value of 10% change in resistance) to 100 ppm of an oxidizing agent (NO_2). The recovery of the device baseline resistance is also simple and only requires application of a high energy UV pulse for a short period. Changes in the device resistance in test gas environments were interpreted in terms of a model where the MWCNTs were thought to behave as p-type semiconductors. Charge transfer between the nanotubes and the analyte is an important mechanism in changing the resistance of the sensor when exposed to NH_3 and NO_2.

As part of a comparative study, MWCNTs grown on Si/SiO_2 substrates using an Fe catalyst were integrated into a resistive sensor design and were evaluated for their sensor response. A detailed study was made to improve the device sensitivity by spin coating the nanotube film with polymer composites like PEDOT: PSS and depositing Nano crystalline TiO_2 particles around the nanotubes. Steady state sensitivities as high as 10% and 11% were achieved for 100ppm of NH_3 and NO_2 respectively, at room temperature.

For studying the transport mechanism, metal contacts of area $0.07 cm^2$ were deposited under high vacuum by e-beam evaporation technique on both sides of the template. These devices were characterized for their electrical properties by Current – Voltage (I–V) measurements at room temperature. A typical I-V curve with an ohmic behavior was observed for a device with platinum electrodes deposited on both sides yielding a resistivity value of 100-150 Ω-cm. I–V curves from a CNT device with copper and platinum as top and bottom contact electrodes respectively shows an asymmetrical behavior, which can be attributed to the presence of a Schottky barrier at the Cu/CNT interface. This can also be attributed to better crystallinity of our nanotubes grown through a template assisted method.

Electrical characterization of these devices exhibited a Schottky behavior at room temperature with low work function metal contacts like aluminum and copper and ohmic behavior with high work function metals like Au and Pt. This was also in accordance with the gas sensing experiments performed on these devices indicating a p-type semiconducting behavior of our nanotubes. An extensive study through a series of electrical measurements with various metal contacts, conclusively showed that the nanotubes are electrically semiconducting with resistivity in the range of 100-150 Ω-cm.

Improvements in device designs and optimization of AAO templates and the CVD process are underway to further improve the sensitivity of these MWCNT sensors to various gases. Low temperature I-V measurements are in progress to unequivocally confirm this observed behavior.

References

1. S. Iijima, "Helical Microtubules of Graphitic Carbon," *Nature*, vol. 354, pp. 56-58, 1991.
2. R. H. Baughman, A. A. Zakhidov, and W. A. de Heer, "Carbon nanotubes – the route toward applications," *Science*, vol. 297, pp. 787-792, 2002.
3. Wang, S.G.; Zhang, Q.; Yang, D.J.; Sellin, P.J. and Zhong, G.F. 2004 *Diamond Relat. Mater.* **13**, 1327 (2004).
4. M. Madou, S. Morrison, Chemical sensing with solid state devices, Academic Press,Inc., San Diego, 1989.
5. Kong, J., Franklin, N., Zhou, C., M. Chapline, S. Peng, K. Cho, H. Dai, 2000 *Science*, **287** 622
6. Collins, G.; Bradley, K.; Ishigami, M.; Zettl, A. 2000 *Science* **286** 1801.
7. L. Valentini, I. Armentano, J. Kenny, C. Cantalini, L. Lozzi, S. Santucci, 2003 *Appl. Phys. Lett.* **82** 961
8. J. Li, Y. Lu, Q. Ye, M. Cinke, J. Han, M. Meyyappan, 2003 *Nano Lett.* **3** 929
9. Snow, E. S.; Perkins, F. K.; Houser, S. C.; Badescu, S. C.; Reinecke, T. L. 2005 *Science* **307** 1942.
10. Snow, E.S.; Perkins, F.K. and Robinson, J. A. 2006 Chem. Soc. Rev., **35** 790
11. Modi, A.; Koratkar, N.; Lass, E; Wei, B. and Ajayan, P.M. 2003 Nature **424**, 171
12. Kong, J.; Chapline, M. G. and Dai, H. 2001 *Adv. Mater*. **13**, 1384
13. Valentini, L. ; Armentano, I. ; Kenny, J.M. ; Cantalini, C. ; Lozzi, L. and Santucci, S. 2003 *Appl. Phys. Lett.* **82**, 961
14. Qi, P.; Vermesh, O.; Grecu, M.; Javey, A.; Wang, Q.; Dai, H.; Peng, S. and Cho, K. J. 2003 *Nano Lett.* **3**, 347
15. Wang, S.G.; Zhang, Q.; Yang, D.J.; Sellin, P.J. and Zhong, G.F. 2004 *Diamond Relat. Mater.* **13**, 1327 (2004).
16. Jang, Y.T.; Moon, S.I.; Ahn, J.H.; Lee, Y.H. and Ju, B.K. 2004 Sens. Actuators B **99**, 118

17. Bekyarova, E.; Davis, M.; Burch, T.; Itkis, M. E.; Zhao, B.; Sunshine, S. and Haddon, R.C.; 2004 *J. Phys. Chem. B* **108**, 19717
18. Liang, Y.X.; Chen, Y.J. and Wang, T.H. 2004 *Appl. Phys. Lett.* **85**, 666
19. Raissi, F. and Farivar, R. 2005 Appl. Phys. Lett. **87**, 164101
20. Zhang, J.; Boyd, A.; Tselev, A.; Paranjape, M. and Barbara, P. 2006 Appl. Phys. Lett. **88**, 123112
21. Cho, W. S.; Moon, S. I.; Paek, K. K.; Lee, Y. H.; Park, J. H. and Ju, B. K. 2006 *Sens. Actuators B* **119**, 180
22. Dai, L.; Patil, A.; Gong, X.; Guo, Z.; Liu, L.; Liu, Y.; Zhu, D. 2003 *ChemPhys Chem* **4**, 1150 and references cited therein.
23. He, P.; Dai, L. 2004 *Chem. Commun.* 348 and references cited therein.
24. Wei, Chen; Dai, Liming; Roy, Ajit and Tolle, Tia Benson 2006 *J. Am. Chem. Soc.* **128**, 1412
25. Singh, V.P. Aguilera, A.; Jayaraman, V.; Sanagapalli, S.; Singh, R.S.; Jayaraman, V.; Sampson, K. 2006 *Solar Energy Materials and Solar Cells*, **90**, 713
26. Andrews, R.; Jacques, D.; Rao, A.; Derbyshire, F.; Qian, D.; Fan, X.; Dickey, E.; and Chen, J. 1999 *Chem. Phys. Lett.,* **303**, 467
27. S. J. Tans, A. R. M. Verschueren, and C. Dekker, Nature London393, 49 1998.
28. R. Martel, T. Schmidt, H. R. Shea, T. Hertel, and P. Avouris, Appl. Phys. Lett. 73, 2447 1998.
29. K. Esfarjani, A. A. Farajian, Y. Hashi, and Y. Kawazoe, Appl. Phys. Lett. 74, 79 1999.
30. J. Kong, J. Cao, and H. Dai, Appl. Phys. Lett. 80, 73 2002.
31. Y. Zhou, A. Gaur, S. H. Hur, C. Kocabas, M. A. Meitl, M. Shim, and J. A. Rogers, Nano Lett. 4, 2031 2004.
32. R. D. Antonov and A. T. Johnson, Appl. Phys. Lett. 83, 3274 1999.
33. Z. Yao, H. W. C. Postma, L. Balents, and C. Dekker, Nature London 402, 273 1999.
34. M. Freitag, M. Radosavljevic, Y. Zhou, and A. T. Johnson, Appl. Phys. Lett. 79, 3326 2001.

35. J. U. Lee, P. P. Gipp, and C. M. Heller, Appl. Phys. Lett. 85, 145 2004.
36. H. M. Manohara, E. W. Wong, E. Schlecht, B. D. Hunt, and P. H. Siegel, Nano Lett. 5, 1469 2005.
37. S. Iijima. Helical Microtubules of Graphitic Carbon. *Nature*, 354:56{58, 1991.
38. S. Iijima, Helical microtubules of graphitic carbon, Nature (London) 354 (1991) 56.
39. B.I. Yakobson, C.J. Brabec, J. Bernholc, Nanomechanics of carbon tubes: instabilities beyond linear response, Phys. Rev. Lett. 76 (1996) 2511.
40. N. Hamada, S. Sawada, A. Oshiyama, New one-dimensional conductors: graphitic microtubules, Phys. Rev. Lett. 68 (1992) 1579.
41. W.B. Choi, D.S. Chung, J.H. Kang, H.Y. Kim, Y.W. Jin, I.T. Han, Y.H. Lee, Fully sealed, high-brightness carbon-nanotube fieldemission display, Appl. Phys. Lett. 75 (1999) 3129.
42. S.J. Tans, A.R.M. Verschueren, C. Dekker, Room-temperature transistor based on a single carbon nanotube, Nature 393 (1998) 49.
43. J. Hafner, C. Cheung, C. Lieber, Growth of nanotubes for probe microscopy tips, Nature 398 (1999) 761–762.
44. C. Liu, Y.Y. Fan, M. Liu, H.T. Cong, H.M. Cheng, M.S. Dresselhaus, Hydrogen storage in single-walled carbon nanotubes at room temperature, Science 286 (1999) 1127.
45. S.J. Tans, M.H. Devoret, H. Dai, A. Thess, R.E. Smalley, L.J. Geerligs, C. Dekker, Individual single-wall carbon nanotubes as quantum wires, Nature 386 (1997) 474.
46. C. Niu, E.K. Sichel, R. Hoch, D. Moy, H. Tennent, High power electrochemical capacitors based on carbon nanotube electrodes, Appl. Phys. Lett. 70 (1997) 1480.
47. M. Bienfait, B. Asmussen, M. Johnson, P. Zeppenfeld, Methane mobility in carbon nanotubes, Surf. Sci. 1–3 (2000) 243–248.
48. K.G. Ong, K. Zeng, C.A. Grimes, A wireless passive carbon.

49. J.W.G. WildÄoer, L.C. Venema, A.G. Rinzler, R.E. Smalley, and C. Dekker. Electronic structure of atomically resolved carbon nanotubes. *Nature (London)*, 391:59, 1998.
50. M. Bockrath, D.H. Cobden, P.L. McEuen, N.G. Chopra, A. Zettl, A. Thess, and R.E. Smalley. Single-Electron Transport in Ropes of Carbon Nanotubes. *Science*, 275:1922, 1997.
51. J. Nygºard, D.H. Cobden, and P.E. LindelÄof. Kondo physics in carbon nanotubes. *Nature (London)*, 408:342, 2000.
52. S. Frank, P. Poncharal, Z.L.Wang, and W.A. de Heer. Carbon nanotube quantum resistors. *Science*, 280:1744, 1998.
53. P. Poncharal, C. Berger, Y. Yi, Z.L. Lang, and W.A. de Heer. Room temperature ballistic conduction in carbon nanotubes. *J. Phys. Chem. B*, 106:12104, 2002.
54. A.Y. Kasumov, R. Deblock, M. Kociak, B. Reulet, H. Bouchiat, I.I. Khodos, Yu.B. Gorbatov, V.T. Volkov, C. Journet, and M. Burghard. Carbon nanotubes as molecular quantum wires. *Science*, 284:1508, 1999.
55. M. Kociak, A.Y. Kasumov, S. Gueron, B. Reulet, I.I. Khodos, Y.B. Gor- batov, V.T. Volkov, L. Vaccarini, and H. Bouchiat. Superconductivity in ropes of single-walled carbon nanotubes. *Phys. Rev. Lett.*, 86:2416, 2001.
56. M. M. J. Treacy, T. W. Ebbesen, and J. M. Gibson. Exceptionally High Young's Modulus Observed for Individual Carbon Nanotubes. *Nature*, 381:678{680, June 1996.
57. S. Berber, Y.-K. Kwon, and D. Tomanek. Unusually High Thermal Conductivity of Carbon Nanotubes. *Physical Review Letters*, 84(20):4613{4616, 2000.
58. Nanopedia. http://nanopedia.case.edu/NWPage.php?page=nanotube.chirality.
59. Nanotechnology Now. http://www.nanotech-now.com/nanotube-buckyball-sites.htm.
60. L. Valentini, C. Cantalini, I. Armentano, J.M. Kenny, L. Lozzi, S.Santucci, Diamond Related Mater. 13 (2004) 1301.

61. Huczko, A “Synthesis of aligned carbon nanotubes” Applied Physics A (Materials Science Processing), vol A74, pp 617-38, 2002.
62. Hulteen, J.C. Chen, H.X.; Chambliss, C.K.; Martin, C.R. “Template synthesis of carbon nanotubule and nanofiber arrays” Nanostructured Materials, vol 9, p p 133-136, 1997.
63. J. Kong, N.R. Franklin, C. Zhou, M.G. Chapline, S. Peng, K. Cho, H. Dai, Science 287 (2000) 622.
64. H. Chang, J.D. Lee, S.M. Lee, Y.H. Lee, Appl. Phys. Lett. 79 (2001) 3863.
65. L. Valentini, I. Armentano, J.M. Kenny, C. Cantalini, L. Lozzi, S.Santucci, Appl. Phys. Lett. 82 (2003) 961.
66. W.S. Cho, S.I. Moon, Y. D Lee, Y.H. Lee, J.H. Park, B.K. Ju, IEEE Electron. Dev. Lett. 26 (2005) 498.
67. S. Santucci et al., J. Chem. Phys. 119 (2003) 10904.
68. J. Singh, Semiconductor Devices: Basic Principles Wiley, New York, 2001.
69. J.J. Palacios, A.J. P¶erez-Jim¶enez, E. Louis, E. SanFabi¶an, and J.A. Verg¶es. First-principles phase-coherent transport in metallic nanotubes with realistic contacts. *Phys. Rev. Lett*, 90:6801, 2003.
70. P. Poncharal, C. Berger, Y. Yi, Z.L. Lang, and W.A. de Heer. Room temperature ballistic conduction in carbon nanotubes. *J. Phys. Chem. B*, 106:12104, 2002.
71. P. Avouris, J. Appenzeller, R. Martel, and S. J. Wind, "Carbon nanotube electronics," *Proceedings of the Ieee*, vol. 91, pp. 1772-1784, 2003.
72. S. Heinze, J. Tersoff, R. Martel, V. Derycke, J. Appenzeller, and P. Avouris, "Carbon nanotubes as Schottky barrier transistors," *Physical Review Letters*, vol. 89, pp. 106801.1-106801.4, 2002.
73. J. Guo, S. Datta, and M. Lundstrom, "A numerical study of scaling issues for Schottky-Barrier carbon nanotube transistors," *Ieee Transactions on Electron Devices*, vol. 51, pp. 172-177, 2004.
74. S. J. Wind, J. Appenzeller, R. Martel, V. Derycke, and P. Avouris, "Fabrication and electrical characterization of top gate single-wall carbon nanotube field-effect

transistors," *Journal of Vacuum Science & Technology B*, vol. 20, pp. 2798-2801, 2002.

75. A. Javey, J. Guo, Q. Wang, M. Lundstrom, and H. J. Dai, "Ballistic carbon nanotube field-effect transistors," *Nature*, vol. 424, pp. 654-657, 2003.
76. A. Javey, J. Guo, D. B. Farmer, Q. Wang, E. Yenilmez, R. G. Gordon, M. Lundstrom, and H. Dai, "Self-aligned ballistic molecular transistors and parallel nanotube arrays," *Nano. Lett.*, in press, 2004.
77. R. Martel, V. Derycke, C. Lavoie, J. Appenzeller, K. Chan, J. Tersoff, and P. Avouris, Phys. Rev. Lett. 87, 256805 2001.
78. A. Javey, J. Guo, M. Lundstrom, and H. J. Dai, Nature London424, 654 2003.
79. T. Nakanishi, A. Bachtold, and C. Dekker, Phys. Rev. B 66, 073307 2002.
80. S. A. Knaack, M. Redden and M. Onellion, *"AAO nanopore arrays: A practical entrée to nanostructures"*, American Journal of Physics, 72 (7), p856-859 (2004).
81. Singh, R. Pantarotto, D.; Lacerda, L.; Pastorin, G.; Klumpp, C.; Prato, M.; Bianco, A.; Kostarelos, K. "Tissue biodistribution and blood clearance rates of intravenously administered carbon nanotube radiotracers" *Proc. Natl. Acad. Sci. USA*, vol 103, pp 3357-62, 2006.
82. Singh, V.P. Aguilera, A.; Jayaraman, V.; Sanagapalli, S.; Singh, R.S.; Jayaraman, V.; Sampson, K. "Porous alumina templates and nanostructured CdS for thin film solar cell applications" Solar Energy Materials and Solar Cells, vol 90, pp 713-26, 2006.
83. M. Dresselhaus, G. Dressehqaus, P. Eklund, "Science of Fullerenes and Carbon Nanotubes", Academic, New York, Chapter 19, 1996.
84. Y. C. Sui, D. R. Acosta, J. A. Gonza´lez-Leo´n, A. Bermu´dez, J. Feuchtwanger, B. Z. Cui, J. O. Flores, and J. M. Saniger J. Phys. Chem. B vol 105, pp 1523-1527, 2001.
85. Yuko Kato , Ken-ichi Shimizu , Norimitsu Matsushita , Tomoko Yoshida , Hisao Yoshida, Atsushi Satsuma and Tadashi Hattori. Quantification of aluminium coordinations in alumina and silica–alumina by Al K-edge XANES. , *Physical Chemistry Chemical Physics* DOI: 10.1039/b100610j

86. Linqin Jiang, Lian Gao and Jing Sun “ Production of aqueous colloidal dispersions of carbon nanotubes”, *Journal of Colloid and Interface Science 260 (2003) 89–94*
87. Soumen Jana, Amin Salehi-Khojin, Wei-Hong Zhong, “ Enhancement of fluid thermal conductivity by the addition of single and hybrid nano-additives”, *S. Jana et al. / Thermochimica Acta 462 (2007) 45–55.*
88.] J.G. Smith, J.W. Connell, K.A. Watson, P.M. Danehy, Polymer 46 (2005) 2276–2284.
89. V. Golob, L. Tusek, Dyes Pigments 40 (1999) 211–217.
90. R. Peixoto et al., Light transmission through porcelain, Dent. Mater., 2007, doi:10.1016/j.dental.2006.11.025.
91. Snow, E.S.; Perkins, F.K. and Robinson, J. A. 2006 Chem. Soc. Rev., **35** 790

Vita

Raghu Mangu was born on November 29, 1983 in Visakhapatnam, India. After completing Bachelor of Technology in Electrical and Electronics Engineering from Jawaharlal Nehru University, Hyderabad, India, in 2006, he enrolled for Masters Program in Electrical Engineering at the University of Kentucky in Fall 2006. He, during his Masters program, worked as a researcher in the field of nanotechnology and developed high sensitivity carbon nanotube sensors for gas detection. He was the member of the University of Kentucky Solar Car team which participated in the North American Solar Challenge-08 and finished 11th position.